Structural analysis of MDM2 RING separates degradation from regulation of p53 transcription activity

Koji Nomura, Marta Klejnot, Dominika Kowalczyk, Andreas K. Hock, Gary J. Sibbet, Karen H. Vousden[*#] and Danny T. Huang[*]

Cancer Research-UK Beatson Institute, Garscube Estate, Switchback Road, Glasgow, G61 1BD, United Kingdom.

[#] Current address: The Crick Institute, 1 Midland Road, London NW1 1AT

[*]Correspondence: karen.vousden@crick.ac.uk , d.huang@beatson.gla.ac.uk,

Abstract

MDM2-MDMX complexes bind the p53 tumor suppressor protein, inhibiting p53's transcriptional activity and targeting p53 for proteasomal degradation. Inhibitors that disrupt binding between p53 and MDM2 efficiently activate a p53 response although their use in the treatment of cancers that retain wild type p53 may be limited by on-target toxicities due to p53 activation in normal tissue. Guided by a novel crystal structure of the MDM2-MDMX-E2(UbcH5B)–ubiquitin complex, we designed MDM2 mutants that prevent E2–ubiquitin binding without altering the RING domain structure. These mutants lose MDM2's E3 activity, but retain the ability to limit p53's transcriptional activity and allow cell proliferation. Cells expressing these mutants responded more quickly to cellular stress than cells expressing wild type MDM2. Targeting the MDM2 E3 ligase activity could widen the therapeutic window of p53 activation in tumors, since rapid p53 induction can be achieved while basal p53 control by MDM2 is maintained.

Introduction

The p53 tumor suppressor protein is induced in response to various types of oncogenic stress, functioning to arrest cell proliferation and induce cell death. Numerous mechanisms to control p53 have evolved, with a key role for the related RING domain proteins MDM2 and MDMX. In mice, deletion of either MDM2 or MDMX results in early embryonic lethality due to uncontrolled p53 activation[1-7].

In healthy unstressed cells, MDM2 is primarily localized in the nucleus where it binds and inhibits p53, partly by ubiquitinating p53 and targeting it for proteasomal degradation[8]. The MDM2 RING domain is necessary for ubiquitin ligase (E3) activity and dimerization with itself or the RING domain of MDMX. Although MDMX can homodimerize at micro-molar concentration *in vitro*[9], in cells, MDMX does not homodimerize and possesses no intrinsic E3 activity[10-13]. However, MDM2 and MDMX form an active E3 heterodimer, and some studies suggest this complex is the physiologically relevant ligase. MDM2's E3 activity also contributes to transcriptional repression by ubiquitinating histones within promoters[14]. Furthermore, interactions between MDM2 and p53 can also directly inhibit the transcription factor function of p53 by altering interactions with other components of the transcriptional machinery[15-17]. In addition to a requirement to bind p53, other functions of MDM2 are important for the control of p53 activity.

Mutations that prevent MDM2 RING domain homo- or heterodimerization lead to the loss of E3 activity and a failure to restrain p53 function[6, 7, 18]. The C-terminal tail of MDM2 is also important for E3 activity, although this function can be provided by MDMX *in vitro*[19, 20]. Interestingly, *in vivo* an MDM2 tail mutant controlled p53 activity sufficiently to allow for normal development, despite

accumulation of p53 above basal levels in some tissues[21]. These results suggest that MDM2 can control p53 through degradation-independent mechanisms.

The induction of p53 in response to stress is accompanied by the inhibition of MDM2, leading to the stabilization of transcriptionally active p53. Defects in the ability to inactivate MDM2 are frequently seen in cancers that retain wild type p53, and in which small molecule inhibitors of MDM2 may have a therapeutic benefit[22]. Several drugs that target the binding of p53 to MDM2 have been developed[23-25] and show excellent specificity in stabilizing and activating p53. However, on-target toxicities including thrombocytopenia and neutropenia appear to limit the efficacy and utility of these compounds[26, 27].

Previous studies have shown that the RING domain of MDM2 functions to recruit E2 ubiquitin-conjugating enzyme thioesterified with ubiquitin (E2~Ub; ~ indicates thioester bond) and facilitate ubiquitination[28, 29]. We have solved the crystal structure of MDM2-MDMX RING domain heterodimer bound to E2(UbcH5B) covalently linked to ubiquitin (UbcH5B–Ub; – indicates covalent bond) and generated MDM2 mutants that retain RING domain integrity but do not interact with UbcH5B–Ub. While these mutants are unable to ubiquitinate and degrade p53, they retain the ability to limit p53's activity.

Results

Structure of MDM2-MDMX RING domain bound to UbcH5B–Ub

To understand how MDM2 RING domain binds and activates E2~Ub for catalysis, we assembled both MDM2 RING homodimer ($MDM2^{RH}$; MDM2 428-C) and MDM2-MDMX RING heterodimer ($MDM2^{R}$-$MDMX^{R}$; MDM2 428-C and MDMX 427-C) in complex with UbcH5B–Ub for crystallization. UbcH5B–Ub complex was obtained by mutating UbcH5B's C85 to a lysine to form an isopeptide bond with the C-terminal glycine of Ub[30, 31]. Only $MDM2^{R}$-$MDMX^{R}$-UbcH5B–Ub complex yielded diffracting crystals and the structure was determined to 2.16 Å (**Fig. 1a-c** and **Table 1**).

There are two copies of $MDM2^{R}$-$MDMX^{R}$-UbcH5B–Ub complex in the asymmetric unit (r.m.s deviation of 0.29 Å for Cα atoms). In both copies, $MDM2^{R}$ binds both UbcH5B and Ub whereas $MDMX^{R}$ only contacts Ub via its C-terminal tail (**Fig. 1a-c**). This UbcH5B–Ub binding arrangement is similar to that observed in the structures of other homodimeric RING E3-E2–Ub complexes[31-33]. However, unlike homodimeric RING E3s where two molecules of E2–Ub bind, $MDM2^{R}$-$MDMX^{R}$ only binds one molecule of UbcH5B–Ub because MDMX does not bind UbcH5B–Ub.

Interactions between $MDM2^{R}$-$MDMX^{R}$ and UbcH5B–Ub

The structure of UbcH5B–Ub adopts the closed, "folded back" configuration similar to those observed in other RING E3-E2–Ub complexes[30-37] (**Fig. 1a-c**) suggesting that $MDM2^{R}$-$MDMX^{R}$ primes Ub for transfer. The closed UbcH5B–Ub conformation is stabilized by numerous interactions involving $MDM2^{R}$-UbcH5B, Ub-UbcH5B, $MDM2^{R}$-Ub and Ub-MDMX tail interfaces. The $MDM2^{R}$-UbcH5B

interaction involves UbcH5B's N-terminal helix, L1 and L2 loops and the hydrophobic core of MDM2^{R} centering on I440 (**Fig. 1d**). Ub-UbcH5B interactions include UbcH5B's α2 contacting Ub's I44 surface and UbcH5B's active site residues clamping Ub's C-terminal tail (**Fig. 1e**). MDM2^{R}-Ub interactions involve MDM2's V477 and Zn^{2+}-ligand H457 and Ub's L8/I36/L71 surface. Additionally, MDM2's R479, known as the "linchpin Arg"[38], forms hydrogen bonds with the carbonyl oxygens of UbcH5B's Q92 and Ub's R72 and the sidechain of Ub's Q40 (**Fig. 1f**). These interactions are similar to those observed in other RING E3-E2–Ub complexes[30-37]. MDM2 also contains a short helix that precedes the RING domain, where S429 and N433 from this helix contact Ub's T9/K11 surface (**Fig. 1f**).

We mutated a selection of key residues involved in Ub-UbcH5B (N77A, D87A, S108R, N114A and D117A in UbcH5B, and I44A and L73D in Ub), MDM2^{R}-Ub (N433R, V477A and R479A in MDM2, and T9A, I36A and Q40R in Ub) and MDM2^{R}-UbcH5B (I440A in MDM2) interfaces and performed single-turnover Ub transfer to lysine. All mutants were defective in discharging UbcH5B~Ub suggesting that the observed interactions are important for MDM2-MDMX-catalyzed Ub transfer (**Fig. 1g-i** and **Supplementary Fig. 1a-f**).

The importance of the MDMX C-terminal tail in MDM2-MDMX heterodimer

E3 defective mutations in the C-terminal tail of MDM2 can be reactivated by MDMX[19, 20, 39]. Our structure shows that the last three residues of MDMX (F488-I489-A490) play a crucial role in stabilizing the closed UbcH5B–Ub conformation. F488 packs against Ub's G35 surface and A490 is completely buried within the MDM2^{R}-Ub interface to support Ub binding (**Fig. 2a**). This binding mode suggests

that MDMX's C-terminus cannot accommodate extra residues. Furthermore, the structure shows that MDM2's C-terminal tail does not contact UbcH5B–Ub.

To assess the importance of MDMX's C-terminus, we mutated F488 to histidine and alanine and found both mutants were defective in discharging UbcH5B~Ub (**Fig. 2b,c** and **Supplementary Fig. 1g,h**). Addition of a hexahistidine tag to MDMX's C-terminus also hindered discharge of UbcH5B~Ub (**Fig. 2d** and **Supplementary Fig. 1i,j**). However, substitution of the corresponding C-terminal residue in MDM2, Y489, to histidine or alanine or addition of a hexahistidine tag to MDM2's C-terminus had a minimal effect (**Fig. 2b-d** and **Supplementary Fig. 1g-j**), consistent with our structure. Thus, the length of MDMX's C-terminus impacts E2~Ub recruitment by MDM2-MDMX heterodimer. MDMX's F488-Ub interaction is conserved in homodimeric RING E3s such as RNF4 and BIRC7[31-33] but in these examples the C-terminus is only partially buried and introducing exogenous C-terminal residues minimally affected activity[40].

A model for MDM2 homodimer bound to E2~Ub

Given that MDMX only contributes to the tail-Ub interaction, we reasoned that MDM2's C-terminus could fulfill this role in the MDM2 homodimer. Indeed, substituting MDMX's C-terminal F488-I489-A490 with MDM2's C-terminal Y489-F490-P491 marginally improved MDM2-MDMX's activity (**Fig. 2c** and **Supplementary Fig. 1g,h**) suggesting that the MDM2 homodimer likely uses a similar mechanism to activate E2~Ub. Since MDM2 and MDMX RING domain structures are similar (r.m.s. deviation of 0.44 Å for Cα atoms) and the NMR structure of $MDM2^{RH}$ [29] is similar to $MDM2^{R}$-$MDMX^{R}$ (r.m.s. deviation of 1.47 Å for Cα atoms), we generated a model of $MDM2^{RH}$ bound to UbcH5B–Ub by

superimposition of MDM2^{R}-UbcH5B–Ub from our structure onto MDMX^{R} in the MDM2^{R}-MDMX^{R}-UbcH5B–Ub structure (**Fig. 3a,b**). In this model, each MDM2 RING domain binds one molecule of UbcH5B–Ub and their C-terminal tails are buried within the adjacent MDM2^{R}-Ub interface to support Ub binding.

To validate this model, we mutated a selection of key residues in the Ub-UbcH5B (UbcH5B S108R and Ub I44A), MDM2^{R}-Ub (MDM2 R479A) and Ub-MDM2 tail (MDM2 Y489A) binding interface and performed UbcH5B~Ub discharge assay catalyzed by MDM2 homodimer. All mutants were defective in discharging UbcH5B~Ub. Moreover, addition of a C-terminal hexahistidine tag reduced the activity (**Fig. 3c** and **Supplementary Fig. 1k,l**). Thus, the MDM2 homodimer uses a similar mechanism as the MDM2-MDMX heterodimer to activate E2~Ub for catalysis.

MDM2 homodimer exhibits higher intrinsic ligase activity

The structure of the MDM2^{R}-MDMX^{R}-UbcH5B–Ub complex shows that the MDM2-MDMX heterodimer can only recruit one molecule of UbcH5B–Ub at a time while the model of the MDM2^{RH}-UbcH5B–Ub complex suggests that the MDM2 homodimer can bind two molecules of UbcH5B–Ub and perhaps enable transfer of two Ub molecules simultaneously. To investigate MDM2^{RH} and MDM2^{R}-MDMX^{R} Ub transfer mechanisms, we compared their rate of UbcH5B~Ub discharge. Because the MDM2 RING domain is known to form large oligomers and dimers during expression and purification from *E. coli*[20], we developed a protocol to purify the dimeric fraction of MDM2 RING domain and then performed UbcH5B~Ub discharge assay by using fluorescently-labeled Ub for quantification. At the same E3 concentration, MDM2^{RH} discharged UbcH5B~Ub at a faster rate as compared to

$MDM2^{R}$-$MDMX^{R}$. When $MDM2^{RH}$ concentration is halved, it displayed a similar rate of UbcH5B~Ub discharge as $MDM2^{R}$-$MDMX^{R}$ (**Fig. 3d,e**). Thus, $MDM2^{RH}$ displays two-fold enhancement in rate as compared to $MDM2^{R}$-$MDMX^{R}$.

Engineering MDM2 RING domain lacking ligase activity

So far, most studies on MDM2's ligase-independent regulation of p53 are based on MDM2 C464A (or C462A in mouse), a mutant that disrupts the Zn^{2+}-coordination[18, 41-43]. This mutation has severe consequences on the RING domain fold and hence the ability to homo- or heterodimerize. We sought to design an MDM2 RING mutant that abrogates the ligase activity while maintaining the RING domain fold to study the ligase independent function of MDM2. Our structure and model suggest that disrupting the $MDM2^{R}$-UbcH5B, $MDM2^{R}$-Ub or MDM2 tail-Ub interaction could hamper the ligase activity. Given that MDM2 tail mutants can be reactivated by MDMX[20, 44], we focused on the $MDM2^{R}$-UbcH5B and $MDM2^{R}$-Ub interfaces. MDM2 I440 and R479 were chosen because I440 plays the central role in E2-binding and R479 helps stabilize the closed E2~Ub conformation. The corresponding residue to I440 in BRCA1, I26, has been mutated to alanine and was found to be defective in activity *in vitro*[45, 46].

We mutated MDM2 I440 and R479 to several different amino acid residues (I440E, I440A, I440D, I440Y, I440R, I440K, R479A, R479P, R479I, R479G, R479F and R479K). The basic and acidic residues are expected to severely impact $MDM2^{R}$-UbcH5B hydrophobic interactions whereas residues with no or short sidechains should not support interactions initiated by the linchpin Arg. *In vitro* UbcH5B~Ub discharge and UbcH5B–Ub binding assays showed that all MDM2 mutants were defective in discharging UbcH5B~Ub compared to the wild type MDM2

(**Supplementary Fig. 2a**). Most I440 variants had no measurable UbcH5B–Ub binding affinity except I440Y, which displayed ~60-fold weaker affinity than the wild type MDM2 (**Supplementary Table 1** and **Supplementary Fig. 3a**). All R479 variants bound UbcH5B–Ub with weaker affinities and only R479P mutant displayed no measurable binding affinity (**Supplementary Table 1** and **Supplementary Fig. 3a**). Consistent with UbcH5B–Ub binding properties, MDM2 mutants that exhibited no measurable UbcH5B–Ub binding affinity were severely compromised in their p53 ubiquitination activity in cells, with MDM2 I440K, I440E and R479P mutants showing basal p53 ubiquitination levels similar to the empty vector (EV) while MDM2 I440A, I440R and I440D displaying trace p53 ubiquitination activity (**Fig. 4a, b**).

Based on these results, MDM2 I440K, I440E and R479P were selected for subsequent analyses. To verify these mutations do not have an impact on MDM2 homo- or heterodimerization, we performed pull-down experiments *in vitro*. All GST-tagged MDM2 variants were able to pull-down their corresponding His-tagged MDM2 and MDMX variants, suggesting that these mutants are competent in forming MDM2 homodimers and MDM2-MDMX heterodimers (**Supplementary Fig. 2b,c**).

Immunoprecipitation results show that all the I440 and R479 mutants retained the ability to interact with MDMX in cells (**Fig. 4c**), while the negative control MDM2 C464A did not show any interaction. These results were confirmed by showing that wild type MDM2, I440K and I440E mutants can interact with and import MDMX into the nucleus (**Fig. 4d**), while C464A did not relocalize MDMX. As expected, all mutants, including C464A mutant, interacted with p53 (**Fig. 4e**), showing that neither an intact RING domain nor the ability of MDM2 to interact with the E2~Ub complex is required for the N-terminus of MDM2 to bind to p53.

Furthermore, addition of MDMX did not complement the loss of activity in MDM2 I440K or I440E mutants whereas the defective MDM2 Y489D tail-Ub interaction can be restored with MDMX's tail in the heterodimer (**Fig. 4f** and **Supplementary Fig. 2d**). Together, these results showed that MDM2 I440K, I440E and R479P retain the RING domain fold to form homodimers and heterodimers with MDMX, but cannot interact with E2~Ub to catalyze ubiquitination.

MDMX RING domain is not optimized for E2~Ub activation

To understand the basis for the lack of activity in MDMX we superimposed the structure of $MDMX^R$ onto $MDM2^R$ in our $MDM2^R$-$MDMX^R$-UbcH5B–Ub structure to generate a model of $MDMX^R$-UbcH5B–Ub complex. The model showed that $MDMX^R$ harbors residues that are less optimal in UbcH5B and Ub binding compared to $MDM2^R$ (**Fig. 5a,b**). Strikingly, $MDMX^R$ lacks the linchpin Arg, and instead contains K478, which cannot initiate the same hydrogen bond network as MDM2's R479. Furthermore, the $MDMX^R$-$MDMX^R$ dimerization interface is suboptimal: the two $MDMX^R$ N448 sidechains at this interface potentially clash or create an electrostatic repulsion (**Fig. 5c**). MDM2 contains C449 at this position that does not clash with C449 in the MDM2 homodimer model or MDMX's N448 in MDM2-MDMX heterodimer (**Fig. 5d,e**).

We wondered whether substituting N448C and K478R could reactivate MDMX's ligase activity. A similar MDMX mutant harboring N448C with residues 465-480 replaced with MDM2 sequence was previously shown to promote p53 ubiquitination and degradation in cells[13]. MDMX displayed no activity under the reaction conditions of our UbcH5B~Ub discharge assay, MDMX N448C showed marginal activity, while MDMX K478R massively improved the activity. The

MDMX N448C K478R mutant further enhanced the activity (**Fig. 5f**). To assess whether these MDMX variants are active in cells, we performed p53 ubiquitination assays by transfecting p53, full-length MDMX variants and His-Ub into U2OS cells. MDMX N448C and MDMX K478R exhibited no appreciable activity while MDMX N448C K478R displayed modest p53 ubiquitination activity, compared to full-length MDM2. Remarkably, when we generated an MDM2-MDMX chimera by replacing MDM2's RING domain with MDMX's RING domain (1-421: MDM2, 422-490: MDMX, "MDM2_XRING") to avoid the complications of the lack of NLS and NES and a shorter acidic domain in MDMX, the N448C K478R mutant exhibited p53 ubiquitination activity similar to wild type MDM2 (**Fig. 5g**). Based on the model of active E3 dimers, the MDM2 I440 and R479 mutants, which have lost the ability to bind E2~Ub, may regain E3 activity by forming a dimer with a binding partner - like MDMX or other MDM2 proteins - that retain the ability to bind to the E2~Ub complex. To test this hypothesis, MDMX K478R (not chimera) was co-expressed with MDM2 I440 mutants. All mutants were reactivated by MDMX K478R but not by wild type MDMX (**Fig. 5h**) and binding analysis showed that MDMX K478R has acquired the ability to interact with the UbcH5B–Ub complex (**Supplementary Fig. 3b**). The ability of MDMX K478R to bind E2~Ub and dimerize with MDM2 I440 mutants allows it to ubiquitinate p53 (**Fig. 5i**). Together, these results showed that MDMX RING domain sequence is not optimized for E2~Ub activation and highlighted the importance of the linchpin Arg in regulating the ligase activity. Moreover, these results are consistent with earlier findings that demonstrated the requirement of MDM2 acidic domain in promoting p53 ubiquitination and degradation in cells[47-49].

MDM2 I440 or R479 mutants limit p53 activity

To assess the effect of the MDM2 mutants on endogenous p53, we generated U2OS cells that were conditionally depleted p53 through use of a doxycycline inducible shRNA, then removed endogenous MDM2 from these cells by CRISPR/Cas9 followed by stable re-expression of various MDM2 mutants (**Supplementary Fig. 4a-c**). Removal of doxycycline then allowed for the re-expression of endogenous p53. Expression of wild type MDM2 in this system resulted in a clear degradation of p53 compared to EV transfected cells, while – as expected - the C464A, I440K, I440E and R479P mutants failed to degrade p53 (**Fig. 6a,b**). Interestingly, however, despite failing to target p53 for degradation, the expression of the I440 or R479 mutants resulted in a significantly lower activation of the p53 target genes including p21, PIG3 and TIGAR, compared to that seen in cells expressing the MDM2 C464A mutant (**Fig. 6a,b**, **Fig. 7a**, and **Supplementary Fig. 5**).

Chromatin immunoprecipitation (ChIP) assays to look for MDM2 at the p21 promoter showed that although wild type MDM2 expression reduced the overall amount of p53 protein, the ratio of p53 to MDM2 at the p21 promoter suggested that low levels of both proteins were present. By contrast, although MDM2 C464A retained the ability to interact with p53 when co-precipitated in solution (**Fig. 4e**), this interaction was not maintained at the p21 promoter, explaining why MDM2 C464A cannot efficiently limit p53 activity. Interestingly, the I440 and R479 mutants were all found at the p21 promoter with p53 (**Fig. 6c,d**), suggesting that their ability to limit p53's transcriptional activity reflects a direct perturbation of the formation of an active transcriptional complex at the promoter. In terms of proliferation, in the absence of p53 (with doxycycline) all of the cell lines grew at the same rate (**Fig. 6e**). However, following reintroduction of endogenous p53, control cells (lacking MDM2)

stopped growing while cells expressing wild type MDM2 continued proliferating (**Fig. 6e**). Importantly, despite not targeting p53 for degradation, the ability of the MDM2 I440 or R479 mutants to restrain p53 activity was sufficient to allow proliferation of these cells (**Fig. 6e**).

Next, we monitored the response of cells expressing the I440 or R479 MDM2 mutants to stress signals that lead to the dissociation of the p53-MDM2 interaction. While low levels of Actinomycin D inhibit MDM2 by disrupting nucleoli and releasing ribosomal proteins that bind an inhibit MDM2[50, 51], we used 10 nM Actinomycin D, which leads to the phosphorylation of N-terminal residues of p53 and loss of MDM2 binding[52, 53] (**Supplementary Fig. 4d**). Although the expression of the MDM2 I440 or R479 mutants restrained the activation of p53 target genes similarly to the expression of wild type MDM2, cells expressing MDM2 I440 or R479 mutants responded more robustly to a 18 hour treatment of Actinomycin D (**Fig. 7a-c** and **Supplementary Fig. 6**), leading to a higher expression of p53 target genes than that seen in cells expressing wild type MDM2 at this time. As expected, Actinomycin D increased p53 levels in cells expressing wild type MDM2, but did not affect the higher p53 levels in cells expressing the E3 defective MDM2 I440, R479 or C464A mutants (**Fig. 7b,c**). As previously reported[54, 55], stabilization of p53 was accompanied by a decrease in MDMX levels – a response that was only evident in cells expressing wild type MDM2, but not the E3 defective mutant. A time course of the response showed that the lack of requirement to stabilize p53 in cells expressing MDM2 I440 or R479 correlated with a more rapid increase in expression of p21 and PIG3 after Actinomycin D treatment compared to a more gradual increased seen in cells expressing MDM2 wild type (**Fig. 7b,c**). Similar results were obtained in cells treated with two other inhibitors of the p53-MDM2 interaction, Nutlin

(**Supplementary Fig. 6b**) and Doxorubicin (**Supplementary Fig. 6c**). Consistently, cells expressing MDM2 I440 or R479 mutants showed a more rapid attenuation of cell growth in response to Actinomycin D than cells with wild type MDM2 (**Fig. 7d,e**). Therefore, although these MDM2 mutants are unable to control p53 levels, they can still repress p53 activity Moreover, the high levels of p53 in cells expressing these MDM2 mutants can be more rapidly activated in response to stress than p53 controlled by wild type MDM2 (which degrades p53), where the p53 protein must still accumulate.

Discussion

The ability of MDMX to interact with MDM2 through the RING domain has been described to both inhibit or enhance MDM2 E3 ligase activity[10, 56, 57]. Our present work provides the structural and mechanistic insights into how MDM2 homodimer and MDM2-MDMX heterodimer bind and activate E2~Ub for transfer. Both the MDM2 homodimer and MDM2-MDMX heterodimer utilize a similar mechanism as other RING E3s reported previously[30-38, 58], where MDM2 RING-E2, MDM2-Ub and Ub-E2 interactions restrain E2~Ub into a closed conformation that optimally positions the E2~Ub thioester bond for transfer. Complementing previous studies[19, 20, 39], we show that the C-terminal tail of MDM2 and MDMX in the MDM2 homodimer and MDM2-MDMX heterodimer, respectively, and their lengths play a critical role in supporting Ub binding. *In vivo,* a similar C-terminal tail mutant of MDM2 was able to control p53 to allow normal development through a mechanism that required MDMX heterodimerization[21]. Surprisingly, although this complex retains E3 activity, p53 protein accumulated in some tissues and cells from these mice, suggesting that degradation was compromised. While the mechanism of how this C-terminal mutant controls p53 under these conditions remains unclear, these data are consistent with our observations that MDM2 shows E3 independent functions to regulate p53.

Our data indicate that despite their apparent structural similarity, MDM2 homodimer and MDM2-MDMX heterodimer have different ability to transfer Ub due to their ability to interact with E2~Ub complexes, and that MDM2 homodimer exhibits higher intrinsic ligase activity than MDM2-MDMX heterodimer. This can be attributed to the inability of MDMX to recruit E2~Ub therefore halving the amount of E2~Ub recruited by a heterodimer (compared to an MDM2 homodimer) or the

MDM2 RING domain exhibiting a higher turnover rate in the context of the MDM2 homodimer. However, the experiments performed here are based on the RING domain and the regulation of these complexes by post-translational modification[59], other domains[9, 60] or other protein partners which could favor the activity of the MDM2-MDMX heterodimer.

Consistent with an earlier study showing that replacement of MDMX's N448 and residues 465-480 with MDM2's sequences was able to stimulate MDMX's ligase activity[13], we found that substituting MDMX's N448 and K478 to cysteine and arginine, respectively, were sufficient to unmask its ligase activity. The N448C mutation enables RING domain homodimerization, thereby allowing MDMX tail-Ub interaction, whereas K478R presumably stabilizes the closed E2~Ub conformation as observed in our structure. These results further underscore the importance of C-terminal tail-Ub interaction and the linchpin Arg in modulating the ligase activity.

Prior studies have used MDM2 C464A mutant to assess ligase-independent functions in regulating p53, but C464A also abolishes the RING domain fold. It is therefore not clear whether failure of this mutant (or the mouse equivalent) to control p53[18] reflects a loss of E3 function, a loss of dimerization or a failure to bind to p53 at promoters. We show that MDM2 I440K, I440E and R479P abrogate the interaction with E2~Ub complexes and abolish MDM2's E3 activity, while retaining the ability to interact with p53, and to homodimerize or heterodimerize (with MDMX), suggesting they retain an intact RING domain fold. These mutants can be localized on p21 promoter (via p53) and efficiently reduce p53's transcriptional activity, allowing proliferation but rendering cells hypersensitive to stress. Interestingly, MDM2 C464A also retains some effect on cell growth and modestly limits the induction of p53 target genes including p21 (**Fig. 6a,b**), potentially reflecting the ability of this mutant to

bind p53 in solution (a summary of the activity of these MDM2 mutants is available in **Supplementary Table 2**).

Finally, it is possible that targeting the catalytic activity of MDM2 to reactivate wild type p53 in tumors (which have elevated levels of stress) could open a therapeutic window by avoiding the deleterious on-target side effects of completely disrupting the MDM2-p53 interaction in normal tissue. Previous work has described small molecule inhibitors of MDM2 that bind to the RING domain, inhibiting the E3 activity and stabilizing p53[61], suggesting that such an approach is feasible.

Data availability

Coordinates and structure factors for MDM2-MDMX-UbcH5B–Ub complex have been deposited in Protein Data Bank under accession code of 5MNJ. All other data are available from the corresponding authors upon reasonable request.

Acknowledgements

We would like to thank Lori Buetow for her comments on the manuscript; DLS for access to beamlines I24 beamlines (mx8659) that contributed to the results presented here. This work was supported by Cancer Research UK and D.T.H was supported by European Research Grant (grant number 647849).

Authors' contributions

K.N., A.K.H. and K.H.V designed cell-based experiments. K.N. performed all cell-based experiments and analyzed the data. M.K. and D.T.H. performed crystallization and structural determination. M.K., D.K. and D.T.H performed protein purification and *in vitro* biochemical assays. G.J.S. performed and analyzed SPR experiments. K.N., A.K.H., K.H.V. and D.T.H wrote the manuscript. All authors read and approved the final manuscript.

References

1. Jones, S.N., Roe, A.E., Donehower, L.A. & Bradley, A. Rescue of embryonic lethality in Mdm2-deficient mice by absence of p53. *Nature* **378**, 206-208 (1995).
2. Montes de Oca Luna, R., Wagner, D.S. & Lozano, G. Rescue of early embryonic lethality in mdm2-deficient mice by deletion of p53. *Nature* **378**, 203-206 (1995).
3. Finch, R.A. *et al.* mdmx is a negative regulator of p53 activity in vivo. *Cancer Res* **62**, 3221-3225 (2002).
4. Migliorini, D. *et al.* Mdm4 (Mdmx) regulates p53-induced growth arrest and neuronal cell death during early embryonic mouse development. *Molecular and cellular biology* **22**, 5527-5538 (2002).
5. Parant, J. *et al.* Rescue of embryonic lethality in Mdm4-null mice by loss of Trp53 suggests a nonoverlapping pathway with MDM2 to regulate p53. *Nat Genet* **29**, 92-95 (2001).
6. Huang, L. *et al.* The p53 inhibitors MDM2/MDMX complex is required for control of p53 activity in vivo. *Proc Natl Acad Sci U S A* **108**, 12001-12006 (2011).
7. Pant, V., Xiong, S., Iwakuma, T., Quintas-Cardama, A. & Lozano, G. Heterodimerization of Mdm2 and Mdm4 is critical for regulating p53 activity during embryogenesis but dispensable for p53 and Mdm2 stability. *Proc Natl Acad Sci U S A* **108**, 11995-12000 (2011).
8. Moll, U.M. & Petrenko, O. The MDM2-p53 interaction. *Mol Cancer Res* **1**, 1001-1008 (2003).
9. Bista, M., Petrovich, M. & Fersht, A.R. MDMX contains an autoinhibitory sequence element. *Proceedings of the National Academy of Sciences of the United States of America* **110**, 17814-17819 (2013).
10. Jackson, M.W. & Berberich, S.J. MdmX protects p53 from Mdm2-mediated degradation. *Molecular and cellular biology* **20**, 1001-1007 (2000).
11. Stad, R. *et al.* Mdmx stabilizes p53 and Mdm2 via two distinct mechanisms. *EMBO Rep* **2**, 1029-1034 (2001).
12. Badciong, J.C. & Haas, A.L. MdmX is a RING finger ubiquitin ligase capable of synergistically enhancing Mdm2 ubiquitination. *Journal of Biological Chemistry* **277**, 49668-49675 (2002).
13. Iyappan, S. *et al.* Turning the RING Domain Protein MdmX into an Active Ubiquitin-Protein Ligase. *Journal of Biological Chemistry* **285**, 33065-33072 (2010).
14. Minsky, N. & Oren, M. The RING domain of Mdm2 mediates histone ubiquitylation and transcriptional repression. *Molecular cell* **16**, 631-639 (2004).
15. Shi, D. & Gu, W. Dual Roles of MDM2 in the Regulation of p53: Ubiquitination Dependent and Ubiquitination Independent Mechanisms of MDM2 Repression of p53 Activity. *Genes & cancer* **3**, 240-248 (2012).
16. Momand, J., Zambetti, G.P., Olson, D.C., George, D. & Levine, A.J. The mdm-2 oncogene product forms a complex with the p53 protein and inhibits p53-mediated transactivation. *Cell* **69**, 1237-1245 (1992).

17. Oliner, J.D. *et al.* Oncoprotein MDM2 conceals the activation domain of tumour suppressor p53. *Nature* **362**, 857-860 (1993).
18. Itahana, K. *et al.* Targeted inactivation of mdm2 RING finger e3 ubiquitin ligase activity in the mouse reveals mechanistic insights into p53 regulation. *Cancer cell* **12**, 355-366 (2007).
19. Uldrijan, S., Pannekoek, W.J. & Vousden, K.H. An essential function of the extreme C-terminus of MDM2 can be provided by MDMX. *EMBO J* **26**, 102-112 (2007).
20. Poyurovsky, M.V. *et al.* The Mdm2 RING domain C-terminus is required for supramolecular assembly and ubiquitin ligase activity. *Embo Journal* **26**, 90-101 (2007).
21. Tollini, L.A., Jin, A., Park, J. & Zhang, Y. Regulation of p53 by Mdm2 E3 ligase function is dispensable in embryogenesis and development, but essential in response to DNA damage. *Cancer cell* **26**, 235-247 (2014).
22. Khoo, K.H., Verma, C.S. & Lane, D.P. Drugging the p53 pathway: understanding the route to clinical efficacy. *Nat Rev Drug Discov* **13**, 217-236 (2014).
23. Shangary, S. *et al.* Temporal activation of p53 by a specific MDM2 inhibitor is selectively toxic to tumors and leads to complete tumor growth inhibition. *Proc Natl Acad Sci U S A* **105**, 3933-3938 (2008).
24. Vassilev, L.T. *et al.* In vivo activation of the p53 pathway by small-molecule antagonists of MDM2. *Science* **303**, 844-848 (2004).
25. Ding, Q. *et al.* Discovery of RG7388, a potent and selective p53-MDM2 inhibitor in clinical development. *J Med Chem* **56**, 5979-5983 (2013).
26. Andreeff, M. *et al.* Results of the Phase I Trial of RG7112, a Small-Molecule MDM2 Antagonist in Leukemia. *Clin Cancer Res* **22**, 868-876 (2016).
27. Ray-Coquard, I. *et al.* Effect of the MDM2 antagonist RG7112 on the P53 pathway in patients with MDM2-amplified, well-differentiated or dedifferentiated liposarcoma: an exploratory proof-of-mechanism study. *Lancet Oncol* **13**, 1133-1140 (2012).
28. Linke, K. *et al.* Structure of the MDM2/MDMX RING domain heterodimer reveals dimerization is required for their ubiquitylation in trans. *Cell Death Differ* **15**, 841-848 (2008).
29. Kostic, M., Matt, T., Martinez-Yamout, M.A., Dyson, H.J. & Wright, P.E. Solution structure of the Hdm2 C2H2C4 RING, a domain critical for ubiquitination of p53. *Journal of Molecular Biology* **363**, 433-450 (2006).
30. Dou, H., Buetow, L., Sibbet, G.J., Cameron, K. & Huang, D.T. Essentiality of a non-RING element in priming donor ubiquitin for catalysis by a monomeric E3. *Nat Struct Mol Biol* **20**, 982-986 (2013).
31. Plechanovova, A., Jaffray, E.G., Tatham, M.H., Naismith, J.H. & Hay, R.T. Structure of a RING E3 ligase and ubiquitin-loaded E2 primed for catalysis. *Nature* **489**, 115-120 (2012).
32. Dou, H., Buetow, L., Sibbet, G.J., Cameron, K. & Huang, D.T. BIRC7-E2 ubiquitin conjugate structure reveals the mechanism of ubiquitin transfer by a RING dimer. *Nat Struct Mol Biol* **19**, 876-883 (2012).
33. Branigan, E., Plechanovova, A., Jaffray, E.G., Naismith, J.H. & Hay, R.T. Structural basis for the RING-catalyzed synthesis of K63-linked ubiquitin chains. *Nat Struct Mol Biol* **22**, 597-602 (2015).

34. Buetow, L. *et al.* Activation of a primed RING E3-E2-ubiquitin complex by non-covalent ubiquitin. *Mol Cell* **58**, 297-310 (2015).
35. Koliopoulos, M.G., Esposito, D., Christodoulou, E., Taylor, I.A. & Rittinger, K. Functional role of TRIM E3 ligase oligomerization and regulation of catalytic activity. *EMBO J* (2016).
36. Sanchez, J.G. *et al.* Mechanism of TRIM25 Catalytic Activation in the Antiviral RIG-I Pathway. *Cell Reports* **16**, 1315-1325 (2016).
37. Scott, D.C. *et al.* Structure of a RING E3 trapped in action reveals ligation mechanism for the ubiquitin-like protein NEDD8. *Cell* **157**, 1671-1684 (2014).
38. Pruneda, J.N. *et al.* Structure of an E3:E2~Ub complex reveals an allosteric mechanism shared among RING/U-box ligases. *Mol Cell* **47**, 933-942 (2012).
39. Dolezelova, P., Cetkovska, K., Vousden, K.H. & Uldrijan, S. Mutational analysis of Mdm2 C-terminal tail suggests an evolutionarily conserved role of its length in Mdm2 activity toward p53 and indicates structural differences between Mdm2 homodimers and Mdm2/MdmX heterodimers. *Cell cycle (Georgetown, Tex.)* **11**, 953-962 (2012).
40. Plechanovova, A. *et al.* Mechanism of ubiquitylation by dimeric RING ligase RNF4. *Nat Struct Mol Biol* **18**, 1052-1059 (2011).
41. Honda, R., Tanaka, H. & Yasuda, H. Oncoprotein MDM2 is a ubiquitin ligase E3 for tumor suppressor p53. *Febs Letters* **420**, 25-27 (1997).
42. Kubbutat, M.H.G., Ludwig, R.L., Levine, A.J. & Vousden, K.H. Analysis of the degradation function of Mdm2. *Cell Growth & Differentiation* **10**, 87-92 (1999).
43. Geyer, R.K., Yu, Z.K. & Maki, C.G. The MDM2 RING-finger domain is required to promote p53 nuclear export. *Nature Cell Biology* **2**, 569-573 (2000).
44. Zheng, N., Wang, P., Jeffrey, P.D. & Pavletich, N.P. Structure of a c-Cbl-UbcH7 complex: RING domain function in ubiquitin-protein ligases. *Cell* **102**, 533-539 (2000).
45. Brzovic, P.S. *et al.* Binding and recognition in the assembly of an active BRCA1 /BARD1 ubiquitin-ligase complex. *Proceedings of the National Academy of Sciences of the United States of America* **100**, 5646-5651 (2003).
46. Christensen, D.E., Brzovic, P.S. & Klevit, R.E. E2-BRCA1 RING interactions dictate synthesis of mono- or specific polyubiquitin chain linkages. *Nature Structural & Molecular Biology* **14**, 941-948 (2007).
47. Meulmeester, E. *et al.* Critical role for a central part of Mdm2 in the ubiquitylation of p53. *Molecular and cellular biology* **23**, 4929-4938 (2003).
48. Argentini, M., Barboule, N. & Wasylyk, B. The contribution of the acidic domain of MDM2 to p53 and MDM2 stability. *Oncogene* **20**, 1267-1275 (2001).
49. Kawai, H., Wiederschain, D. & Yuan, Z.M. Critical contribution of the MDM2 acidic domain to p53 ubiquitination. *Molecular and cellular biology* **23**, 4939-4947 (2003).

50. Dai, M.S. & Lu, H. Inhibition of MDM2-mediated p53 ubiquitination and degradation by ribosomal protein L5. *The Journal of biological chemistry* **279**, 44475-44482 (2004).
51. Dai, M.S. *et al.* Ribosomal protein L23 activates p53 by inhibiting MDM2 function in response to ribosomal perturbation but not to translation inhibition. *Molecular and cellular biology* **24**, 7654-7668 (2004).
52. Choong, M.L., Yang, H., Lee, M.A. & Lane, D.P. Specific activation of the p53 pathway by low dose actinomycin D: a new route to p53 based cyclotherapy. *Cell cycle (Georgetown, Tex.)* **8**, 2810-2818 (2009).
53. Chen, C.S. *et al.* AKT mediates actinomycin D-induced p53 expression. *Oncotarget* **5**, 693-703 (2014).
54. Pan, Y. & Chen, J. MDM2 promotes ubiquitination and degradation of MDMX. *Molecular and cellular biology* **23**, 5113-5121 (2003).
55. Kawai, H. *et al.* DNA damage-induced MDMX degradation is mediated by MDM2. *The Journal of biological chemistry* **278**, 45946-45953 (2003).
56. Linares, L.K., Hengstermann, A., Ciechanover, A., Muller, S. & Scheffner, M. HdmX stimulates Hdm2-mediated ubiquitination and degradation of p53. *Proc Natl Acad Sci U S A* **100**, 12009-12014 (2003).
57. Stad, R. *et al.* Hdmx stabilizes Mdm2 and p53. *The Journal of biological chemistry* **275**, 28039-28044 (2000).
58. Buetow, L. & Huang, D.T. Structural insights into the catalysis and regulation of E3 ubiquitin ligases. *Nature Reviews Molecular Cell Biology* **17**, 626-642 (2016).
59. Cheng, Q. *et al.* Regulation of MDM2 E3 ligase activity by phosphorylation after DNA damage. *Mol Cell Biol* **31**, 4951-4963 (2011).
60. Cheng, Q., Song, T., Chen, L. & Chen, J. Autoactivation of the MDM2 E3 ligase by intramolecular interaction. *Mol Cell Biol* **34**, 2800-2810 (2014).
61. Roxburgh, P. *et al.* Small molecules that bind the Mdm2 RING stabilize and activate p53. *Carcinogenesis* **33**, 791-798 (2012).

Figure legends

Figure 1 Structure of MDM2^{R}-MDMX^{R}-UbcH5B–Ub. (**a**) Cartoon representation of the complex. MDM2^{R} is colored green, MDMX^{R} orange, UbcH5B cyan and Ub yellow. UbcH5B–Ub linkage colored in blue, UbcH5B's α1, L1 and L2 loops, MDM2 and MDMX's C-terminus are indicated. Zinc atoms are depicted in gray sphere. (**b**) Surface representation of the complex, colored and oriented as in **a**. MDMX's C-terminus is indicated with an arrow. (**c**) Schematic drawing of the complex, colored as in **a**. The C-terminal tail of Ub is shown as a black line. Last three residues of MDM2 and MDMX's C-terminal tails (Y489-F490-P491 in MDM2 and F488-I489-A490 in MDMX) are shown as thick dark green and brown lines, respectively. (**d**) Close-up view of MDM2^{R}-UbcH5B interactions. (**e**) Close-up view of Ub-UbcH5B interactions. (**f**) Close-up view of MDM2^{R}-Ub interactions. Left and right panels are related by 90º rotation about the *y* axis. For **d**, **e** and **f**, key residues are shown as sticks and colored as in **a**. Nitrogen and oxygen atoms are in blue and red, respectively. (**g**,**h**) Nonreduced SDS-PAGE showing the discharge of UbcH5B~Ub variants to L-lysine over time catalyzed by MDM2^{R}-MDMX^{R}. Ub's D58 is not involved in the binding interface and D58A substitution had no effect on UbcH5B~Ub discharge. (**i**) Nonreduced SDS-PAGE showing the discharge of UbcH5B~Ub to L-lysine over time catalyzed by MDM2^{R}-MDMX^{R} variants. Uncropped gel images are shown in **Supplementary Data Set 1**.

Figure 2 Importance of MDMX's C-terminal tail. (**a**) Close-up view of MDMX's C-terminal tail. Transparent surface representation was shown. Last three C-terminal residues (F488-I489-A490) are shown as sticks and colored as in **Fig. 1**. (**b**) Schematic drawing of the complex showing disruption in MDMX's C-terminus (left

panel) would hinder the activity whereas disruption in MDM2's C-terminus (right panel) would not have any effect. (**c, d**) Nonreduced SDS-PAGE showing the discharge of UbcH5B~Ub to L-lysine over time catalyzed by $MDM2^{R}$-$MDMX^{R}$ variants. Uncropped gel images are shown in **Supplementary Data Set 1**.

Figure 3 Mechanism of E2~Ub recruitment and activation by $MDM2^{RH}$. (**a**) A model of $MDM2^{RH}$ bound to UbcH5B–Ub generated by superimposition of $MDM2^{R}$-UbcH5B–Ub portion of the structure onto $MDMX^{R}$ in the $MDM2^{R}$-$MDMX^{R}$-UbcH5B–Ub structure. All colorings are as in **Fig. 1**. (**b**) Schematic drawing of the $MDM2^{RH}$-UbcH5B–Ub model in **a**. $MDM2^{RH}$'s C-terminal tails are shown as thick dark green lines. (**c**) Nonreduced SDS-PAGE showing the discharge of UbcH5B~Ub variants to L-lysine over time catalyzed by GST-MDM2 variants. (**d**) Nonreduced SDS-PAGE showing the discharge of fluorescently-labeled UbcH5B~Ub to L-lysine over time catalyzed by $MDM2^{RH}$ and $MDM2^{R}$-$MDMX^{R}$ visualized by InstantBlue (top panel) and LI-COR Odyssey scanner (bottom panel). (**e**) A plot showing the rate of the discharge of fluorescently-labeled UbcH5B~Ub to L-lysine in **d**. The reactions were performed in duplicate. Uncropped gel images are shown in **Supplementary Data Set 1**.

Figure 4 Redesigning ligase-dead MDM2 mutants. (**a, b**) Ubiquitination assay showing that MDM2 I440 or R479 mutants abolish or reduce p53 ubiquitination. (**c**) Co-immunoprecipitation assay showing that, unlike the MDM2 C464A mutant, MDM2 I440K, I440E and R479P can interact with MDMX. (**d**) MDMX is a cytoplasmic protein and can enter nucleus when dimerized with MDM2. GFP-tagged MDMX can be found in the nucleus with MDM2 wild type and I440 mutants,

demomstrating dimerization between the two proteins. This function is lost in the C464A mutant. Scale bar indicates 10 μm. (**e**) Co-immunoprecipitation assay showing all the MDM2 mutants can interact with p53 in solution. An MDM2 protein lacking the p53 binding domain (Δp53BD) was used as a negative control. (**f**) Ubiquitination assay showing that, unlike the C-terminal mutant Y489D, I440 mutants cannot be reactivated by MDMX. Uncropped blot images are shown in **Supplementary Data Set 1**.

Figure 5 Reactivation of MDMX's ligase activity. (**a**) Structural comparison of $MDM2^{R}$-UbcH5B (left panel) and $MDMX^{R}$-UbcH5B (right panel) interface. (**b**) Structural comparison of $MDM2^{R}$-Ub (left panel) and $MDMX^{R}$-Ub (right panel) interface. $MDMX^{R}$-UbcH5B–Ub model was generated by superimposition of $MDMX^{R}$ onto $MDM2^{R}$ in the structure of $MDM2^{R}$-$MDMX^{R}$-UbcH5B–Ub complex. Residues are shown as sticks and all colorings are as in **Fig. 1**. (**c**) A model of $MDMX^{R}$-$MDMX^{R}$ homodimer generated as in **a** showing the presence of N448 at the dimerization interface separated by 2.5 Å. (**d**) A model of $MDM2^{RH}$ generated as in **Fig. 3a** showing the presence of C449 at the dimerization interface separated by 5.0 Å. (**e**) The dimerization interface of $MDM2^{R}$-$MDMX^{R}$ showing MDM2's C449 and MDMX's N448 separated by 3.7 Å. (**f**) Nonreduced SDS-PAGE showing the discharge of UbcH5B~Ub to L-lysine over time catalyzed by $MDM2^{R}$-$MDMX^{R}$ and $MDMX^{R}$ variants at 250 nM (top panel) and 2.5 μM (bottom panel). (**g**) Ubiquitination assay showing the double mutation of N448C and K478R in the MDM2-MDMX chimera (1-421: MDM2, 422-490: MDMX, "MDM2_XRING") is sufficient to reactivate MDMX's E3 ligase activity. (**h**) MDM2 I440 mutants are reactivated by MDMX K478R but not by WT MDMX, reflecting the ability of

MDMX K478R to interact with UbcH5B–Ub complex and ubiquitinate p53. (**i**) Models illustrating that, unlike the MDM2 C-terminus mutant (Y489D), MDM2 I440 mutants cannot be reactivated by wild type MDMX (**Fig. 4f**) because neither MDM2 I440 mutants nor wild type MDMX recruit the UbcH5B–Ub complex (**Supplementary Fig. 3**). However, these mutants can be reactivated by MDMX K478R that binds the UbcH5B–Ub complex (**Fig. 6h and Supplementary Fig. 3**). Red cross indicates the point of mutation. Uncropped gel and blot images are shown in **Supplementary Data Set 1**.

Figure 6 MDM2 I440 and R479 mutants can limit p53 activity. (**a, b**) Western blot analysis showing that although MDM2 I440K, I440E and R479P do not degrade p53, induction of p21 and other p53 target genes is attenuated by these mutants. $n = 3$ independent experiments. p values: v.s. EV (vertical), v.s. C464A (horizontal). n.s. indicates non-significant v.s. EV. (**c**) ChIP for p53 and MDM2 with quantitative PCR for a p53 response element in the p21 promoter (-2350 bp) and a non-specific binding region (+50 bp). $n = 3$ independent experiments (each with 2 technical replicates). p values: v.s. EV (ChIP: p53), v.s. C464A (ChIP: MDM2). (**d**) Ratio of MDM2/p53 on the p21 promoter based on the ChIP (**Fig. 6c**, p21 -2350 No Doxy). MDM2 wild type, MDM2 I440 and R479 mutants were found at the p21 promoter with p53. p values: v.s. wild type (vertical), v.s. C464A (horizontal). (**e**) The inhibition of cell growth seen following restoration of p53 by removal of Doxycycline (Doxy)) in MDM2 knock-out cells was rescued by expressing MDM2 wild type, I440 and R479 mutants. $n = 3$ independent experiments. p values: v.s. C464A. F-statistics and degrees of freedom of ANOVAs are reported in **Supplementary Table 3**. Uncropped blot images are shown in **Supplementary Data Set 1**.

Figure 7 MDM2 I440 and R479 mutants can quickly respond to the stress. (**a**) qPCR showing that expression of the indicated p53 target genes is attenuated by MDM2 I440K, I440E and R479P, and induced more strongly than in cells expressing wild type MDM2 following 18 hours treatment with Actinomycin D (10 nM). $n = 3$ independent experiments. p values: v.s. EV No Doxy (vertical), v.s. wild type No Doxy ActD (horizontal). n.s. indicates non-significant v.s.EV No Doxy. (**b, c**) Examples of immunoblots and quantification of replicate blots showing that p21 and PIG3 are more rapidly induced in cells expressing MDM2 I440 and R479 mutants upon Actinomycin D (10 nM) treatment compared to cells expressing wild type MDM2 $n = 3$ independent experiments. Immunoblots of all samples are available in **Supplementary Fig. 6a**. (**d**) The indicated cells were treated with vehicle or 10nM Actinomycin D for varying times as shown then were fixed and stained 120 hours after plating. Cells expressing MDM2 I440 or R479 mutants more rapidly attenuate cell growth in comparison to MDM2 wild type. (**e**) Quantification of cell growth experiments. SRB intensity was quantified using ImageJ software. p values: v.s. each wild type. n.s. indicates non-significant. $n = 5$ independent experiments. F-statistics and degrees of freedom of ANOVAs are reported in **Supplementary Table 3**. Uncropped blot images are shown in **Supplementary Data Set 1**.

Table 1 Data collection and refinement statistics

	MDM2^{R}-MDMX^{R}-UbcH5B–Ub (PDB: 5MNJ)
Data collection	
Space group	*P1*
Cell dimensions	
a, *b*, *c* (Å)	54.24, 62.76, 66.35
α, β, γ (°)	69.83. 69.22, 78.21
Resolution (Å)	50.5–2.16(2.22–2.16)[a]
R_{merge}	0.075(0.402)
$I/\sigma(I)$	6.8(1.4)
$CC_{1/2}$	0.992(0.73)
Completeness (%)	95.3(93.3)
Redundancy	3.2(2.9)
Refinement	
Resolution (Å)	50.5–2.16
No. reflections	37881
R_{work} / R_{free}	0.190/0.231
No. atoms	
Protein	5318
Ligand/ion (Zn and SO_4)	10
Water	77
B factors	
Protein	55.1
Ligand/ion (Zn and SO_4)	51.7
Water	52.3
R.m.s. deviations	
Bond lengths (Å)	0.008
Bond angles (°)	1.254

[a]Values in parentheses are for highest-resolution shell.

Online Methods

Protein preparation

All constructs were generated by standard PCR-ligation techniques. All proteins are human unless otherwise specified and were expressed in BL21 (DE3) cells or BL21 (DE3) RIL (Stratagene). To generate $MDM2^R$-$MDMX^R$ (MDM2 428-C and MDMX 427-C) for crystallization and assays, $MDM2^R$ and $MDMX^R$ were cloned into the first and second multiple cloning site of a bicistronic vector, RSF_Duet (Novagen), respectively, where $MDM2^R$ contains an N-terminal 6xHis-tag followed by a TEV protease cleavage site. 6xHis-$MDM2^R$-$MDMX^R$ was purified by Ni-NTA affinity, followed by cation exchange and size exclusion chromatography. All $MDM2^R$-$MDMX^R$ variants were purified in the same manner (**Supplementary Fig. 7a**). To generate C-terminal 6xHis-tagged $MDM2^R$-$MDMX^R$ variants, $MDM2^R$ and $MDMX^R$ variants were cloned into pGEX4T1 (GE Healthcare) containing an N-terminal GST-tag and RSF_Duet containing an N-terminal His-tag. $MDM2^R$-$MDMX^R$ variants were formed by co-expressing GST-$MDM2^R$ with His-$MDMX^R$ variants or GST-$MDMX^R$ with His-$MDM2^R$ variants and subsequently purified by Ni-NTA affinity chromatography, followed by glutathione affinity chromatography (**Supplementary Fig. 7b**). For MDMX reactivation and binding assays, $MDMX^R$ variants were cloned into pGEX4T1 containing an N-terminal GST-tag followed by a TEV protease cleavage site. $MDMX^R$ variants were purified by glutathione affinity chromatography for binding analyses or released from the beads by incubation with TEV overnight, followed by cation exchange chromatography for reactivation assays (**Supplementary Fig. 7c**). For binding analyses and assays, MDM2 398-C variants were cloned into pGEX4T1 and purified by glutathione affinity chromatography (**Supplementary Fig. 7d,e**). $MDMX^R$ variants (10 μM; 100 μl) were loaded onto

superdex 75 10/300 to assess their dimerization state (**Supplementary Fig. 7f**). To obtain pure $MDM2^{RH}$ for assay, $MDM2^{R}$ was cloned into pGEX4T1 containing an N-terminal 6xHis-GST-tag followed by a TEV protease cleavage site, expressed in 36 L of *LB broth,* purified by glutathione affinity chromatography and subsequently buffer exchanged into 50 mM Tris-HCl, pH 7.6, 0.4 M NaCl, 5 %(v/v) glycerol and 1 mM DTT. 6xHis-GST tag was removed by incubation with TEV followed by Ni-NTA pass-back. The cleaved $MDM2^{R}$ was further purified by HiLoad 26/600 Superdex 200 chromatography (**Supplementary Fig. 7c** and **Supplementary Fig. 7g**). For ubiquitination assays, *Arabidopsis thaliana* Uba1, UbcH5B variants and Ub variants were prepared as described previously[34]. $UbcH5B^{S22R}$–Ub and UbcH5B–Ub used for crystallization and binding analyses, respectively, were prepared as described previously[34]. To generate fluorescently-labeled Ub, a MHHHHHHCG sequence was inserted at the N-terminus of Ub and purified by Ni-NTA affinity and size exclusion chromatography in PBS buffer, pH 6.6. The protein was labeled by incubation with IRDye® 800CW Maleimide (LI-COR) at a molar ratio of 4:1 (protein:dye) for 2 h at 22 °C in the dark and subsequently buffer exchanged into 25 mM HEPES, pH 7.0 and 150 mM NaCl using a Zeba spin desalting column (Thermo Fisher) to remove excess dye. Protein concentrations were determined by Bio-RAD protein assay using BSA as a standard and Ub concentration was determined as described previously[34]. All MDM2, MDMX and MDM2-MDMX variants were stored in 25 mM Tris-HCl, pH 7.6, 0.4 M NaCl and 1 mM DTT and other proteins were stored in 25 mM Tris-HCl, pH 7.6, 0.15 M NaCl and 1 mM DTT. All plasmids generated for protein expression were described in **Supplementary Table 4.**

Crystallization

MDM2^{R}-MDMX^{R}-UbcH5B–Ub complex was obtained by mixing 6xHis-MDM2^{R}-MDMX^{R} (6.6 mg/ml) and UbcH5B^{S22R}–Ub (20 mg/ml) at a 1:1 molar ratio. Crystals were grown at 19 °C by microseeding using the hanging-drop vapor diffusion method by mixing the complex with an equal volume of reservoir solution containing 0.1 M Tris-HCl, pH 8.5, 0.175 M Li_2SO_4 and 16-20 %(v/v) PEG 3350. The crystals were flash-frozen in 0.1 M Tris-HCl, pH 8.5, 0.175 M Li_2SO_4, 22 %(v/v) PEG 3350 and 20% (v/v) ethylene glycol. Data were collected at beamline I24 at Diamond Light Source (DLS).

Structural determination

The data were integrated with automated XDS[62] and scaled using the CCP4 program suite[63]. Initial phases were obtained by molecular replacement with PHASER[64] using UbcH5B and Ub from PDB 3ZNI[30] and MDM2^{R}-MDMX^{R} from PDB 3VJF[28] as the search models. Two copies of MDM2^{R}-MDMX^{R}-UbcH5B–Ub complex were found in the asymmetric unit. The model was built in COOT[65] and refined using PHENIX[66]. The complex was refined to a resolution of 2.16 Å and the final model contained two copies of UbcH5B (Chains A and E residues 2-147), Ub (Chains B and F residues 1–76), MDM2^{R} (Chains C and G residues 428-491) and MDMX^{R} (Chains D and H residues 427-490). Residues with no observable side chain electron density were built as alanine stub. Details of the refinement statistics are shown in **Table 1**. All figure models were generated using PYMOL (Schrödinger).

Surface Plasmon resonance (SPR) analyses

All SPR experiments were performed at 25 ºC on a Biacore T200 with a CM-5 chip (GE Healthcare). GST-MDM2 398-C and GST-MDMX^{R} variants were coupled

to CM-5 chips as described previously[34]. For GST-MDM2 398-C variants, UbcH5B–Ub variants were serially diluted in running buffer containing 25 mM Tris-HCl, pH 7.6, 150 mM NaCl, 0.1 mg/ml BSA, 1 mM DTT, 0.005% (v/v) Tween-20 and 300 μM UbΔGG. UbΔGG was included to saturate UbcH5B's backside for optimal RING E3-UbcH5B–Ub interaction as described previously[34]. For GST-MDMX^{R} variants, UbcH5B–Ub variants were serially diluted in running buffer containing 25 mM Tris-HCl, pH 7.6, 150 mM NaCl, 0.1 mg/ml BSA, 1 mM DTT and 0.005% (v/v) Tween-20. Binding was measured at indicated concentration ranges in **Supplementary Fig. 3** in duplicate. Data reported are the difference in SPR signal between GST-MDM2 398-C or GST-MDMX^{R} variants and GST alone. The data were analyzed by steady-state affinity analysis using Biacore T200 BIAevaluation software (GE Healthcare) and Scrubber2 (BioLogic Software).

Single-turnover lysine discharge assays

UbcH5B variants (7-10 μM) were charged with Ub variants (20-50 μM) in buffer containing 50 mM Tris-HCl, pH 7.6, 50 mM NaCl, 0.5 μM *Arabidopsis thaliana* UBA1 and 1 mg/ml BSA for 20 min at 23 °C and charging was stopped by incubating the reaction with 0.01 U/ml apyrase (Sigma) and 30 mM EDTA for 2-3 min at 23 °C as described previously[34]. The lysine discharge reactions were then initiated by adding a mixture containing 50 mM Tris-HCl, pH 7.6, 50 mM NaCl, 1 mg/ml BSA, L-lysine (150 mM or 50 mM for **Supplementary Fig. 1**) and E3 variants (as indicated or 0.3 μM in **Figs. 1g-i, 2c,d, 3c** and **Supplementary Fig. 2d**; 0.8 μM in **Supplementary Fig. 1a,c,g,i,k**; 0.6 μM in **Supplementary Fig. 1e**; and 0.25 μM in **Supplementary Fig. 2a**). Final concentrations are in parenthesis. Reactions were quenched with SDS loading buffer at the indicated times, resolved by SDS-PAGE and

visualized by staining with InstantBlue (Expedeon). For quantification in **Supplementary Fig. 1**, the reactions were performed in triplicate. LI-COR Odyssey scanner was used to analyze the stained gels and bands were quantified by using Image Studio Lite software (LI-COR Biosciences). The fraction of UbcH5B~Ub left was plotted on a bar graph. In **Fig. 3d**, Fluorescently-labeled Ub was used instead of Ub and visualization was performed using a LI-COR Odyssey scanner prior to staining with InstantBlue. The fluorescently-labeled UbcH5B~Ub band was quantified by using Image Studio Lite software (LI-COR Biosciences).

***In vitro* pull-down experiments**

GST-MDM2 398-C variants were co-expressed with the respective His-MDM2 398-C variants or His-MDMX 383-C as shown in Supplementary 2b,c. Cells were harvested, lysed and centrifuge. Lysates were applied onto 400 µl of Ni-NTA beads, washed with 25 mM Tris-HCl, pH 7.6, 0.2 M NaCl, 20 mM imidazole and 5 mM β-mercaptoethnaol and eluted with 25 mM Tris-HCl, pH 7.6, 0.2 M NaCl, 200 mM imidazole and 5 mM β-mercaptoethnaol. The eluted product was then applied onto 400 µl of glutathione sepharose beads, washed with 50 mM Tris-HCl, pH 7.6, 0.2 M NaCl, 5 mM DTT and eluted with 50 mM Tris-HCl, pH 7.6, 0.2 M NaCl, 5 mM DTT and 10 mM glutathione. 3 µg of eluted product was then resolved on the SDS-PAGE. For control experiments, GST-MDM2 398-C, His-MDM2 398-C and His-MDMX 383-C were expressed individually. The lysates were divided in half, applied onto 400 µl of Ni-NTA or glutathione sepharose beads, washed and eluted with buffer as above. 3 µg of eluted product or equal volume (for proteins that do not bind the beads, but eluted with the same volume) was then resolved on the SDS-PAGE and visualized by staining with InstantBlue.

Cell culture and generation of tetracycline inducible p53 knockdown-MDM2 knock-out cells

Human osteosarcoma U2OS or human embryonic kidney HEK293 cells were obtained from ATCC and were cultured in Dulbecco's Modified Eagle Medium (DMEM) supplemented with 10 % FBS and 2 mM L-Glutamine. All cell lines were mycoplasma negative and were authenticated by STR multiplex assay.

In the experiments showed in **Fig. 6**, **Fig. 7** and **Supplementary Fig. 4-6**, tetracycline inducible p53 knockdown-MDM2 knock-out cells were used. U2OS cells were infected with pLKO tet-on shRNA targeting p53 and selected by puromycin for 5 days. Knock-down of p53 was confirmed by Western blotting. Doxycycline treatment induced shRNA expression and p53 depletion within 48 hours and this effect was reversed within 5 days after discontinuing doxycycline treatment (**Supplementary Fig. 4a**). CRISPR/Cas9 vectors targeting the MDM2 p53 binding domain was then transiently transfected, clones isolated and CRISPR disruptions assessed by Western blotting, then confirmed genomic PCR followed by DNA sequencing (**Supplementary Fig. 4b,c**).

Doxycycline was discontinued for 5 days before plating for "No Doxy" condition. Plasmids used and target sequences were described in **Supplementary Tables 4 and 5**.

Mutagenesis PCR

Plasmids used are described in **Supplementary Table 4**. All mutations within the RING domain of MDM2 and MDMX were generated by site-directed

mutagenesis using KOD hot start master mix (Cat. No. 71842, Novagen) and verified by DNA sequencing.

Immunoblotting

Cells were washed with PBS and proteins were extracted with lysis buffer (1 % Triton X-100, 150 mM NaCl and 50 mM Tris-HCl pH8.0), which were then centrifuged at 16,100 r.c.f. at 4 °C for 10 minutes. Where appropriate, protein concentration in cellular lysate was determined using the BCA protein assay, with concentrations normalized to the lowest-concentration sample. Samples were heated to 99 °C for 10 minutes with sample buffer (Final concentration: 10 % glycerol, 2 % SDS, 62.5 mM Tris-HCl pH6.8 and 5 % 2-mercaptoethanol) before separation by SDS-PAGE in a 10 % or 4-12 % bis-tris polyacrylamide gel (Life Technologies) and transfer to 0.2 μm nitrocellulose membrane (GE Healthcare). After the transfer, the membrane was blocked by TTBS supplemented with 5 % skimmed milk or Odyssey blocking buffer (LI-COR) for 1 hour, and was then incubated with primary antibodies (**Supplementary Table 6**) overnight at 4 °C.

After this incubation time, the membrane was washed with TTBS and incubated with appropriate secondary antibodies (**Supplementary Table 6**) for 1 hour, then washed with TTBS and TBS, and membrane-bound secondary antibodies were detected using Odyssey scanner (LI-COR). Images were analyzed by Image Studio (LI-COR).

Data were normalized to actin expression, as appropriate.

Immunoprecipitation

Proteins were extracted and normalized as described in immunoblotting section. Cellular lysates containing 250 µg proteins were incubated with 2 µg of appropriate primary antibody (**Supplementary Table 6**) or control IgG for 1 hour at 4 °C, and then incubated with Dynabeads protein G magnetic beads overnight at 4 °C on the rotator. The immunoprecipitates were washed 3 times with PBS and heated to 99 °C for 10 minutes with sample buffer. After removing magnetic beads, SDS-PAGE and membrane transfer were performed as described in immunoblotting section.

Ubiquitination assay

U2OS cells grown in 100 mm dishes were transiently transfected with various plasmids (**Supplementary Table 4**) using Genejuice transfection reagent (Cat. No. 70967, Novagen) and cultivated for further 24 hours. Cells were treated for 5 hours with proteasome inhibitor MG132 (10 mM) and lysed in UBA buffer (6 M Guanidine HCl, 300 mM NaCl and 50 mM phosphate pH 8 supplemented with 100 µg/ml N-Ethylmaleimide (NEM)). Lysates were boiled at 99 °C for 20 minutes with 1,000 RPM shake. His-tag pull-down was performed using 50 µl of Dynabeads His-Tag Isolation & Pull down Beads (Cat. No. 10104D, Novex) overnight and beads were washed with UBA, UBB (3 M Guanidine HCl, 300 mM NaCl and 50 mM phosphate pH 8), UBC (300 mM NaCl and 50 mM phosphate pH 8) then PBS, followed by SDS–PAGE and Western blotting.

Ubiquitinated and input proteins were detected by immunoblotting.

Immunofluorescence

HEK293 cells were grown on 13 mm glass-coverslips (VWR) placed into 6 well plates. Cells were transfected with MDM2 wild type or mutants and GFP-tagged MDMX overnight then washed and fixed with 4 % paraformaldehyde (PFA) (Sigma) in PBS for 20 minutes at room temperature and PFA was quenched with 30 mM glycine in PBS. Cells were washed and permeabilized with 0.2 % Triton X-100 in PBS for 10 minutes at room temperature. Cells were then washed with PBS and blocked with 0.5 % BSA in PBS for 3 hours at room temperature and were then incubated with MDM2 antibody (**Supplementary Table 6**) overnight at 4 °C. After this incubation time, cells were washed with TTBS and incubated with Alexa568-conjugated secondary antibody (**Supplementary Table 6**) for 2 hours, then washed with TPBS and then PBS. Coverslips were washed with double-distilled water to remove any salt residues and then mounted with VECTASHIELD Mounting Medium with DAPI (Vector laboratories). Images were taken using confocal microscope Fluoview FV1000 (Olympus).

RNA Extraction and Quantitative Real-Time PCR

Cells were grown in 100 mm dishes and RNA was extracted using RNeasy Mini Kit (Qiagen) RNA concentration was determined using a Nanodrop 2000c (Thermo Scientific). cDNA was synthesized through reverse transcription polymerase chain reaction (RT-PCR) from 1 μg RNA using High-capacity RNA-to-cDNA Kit (Life Technologies). The quantitative real-time PCR (qPCR) reaction was performed with 10 ng of cDNA using Fast SYBR green master mix. Primers used are described in **Supplementary Table 5.** The amount of fluorescent PCR product accumulating during the PCR programme (20 sec at 95 °C hot start, 40 cycles of 3 sec denaturing at 95 °C, 30 sec annealing-elongation at 60 °C) was detected by the ABI 7500 Fast

(Thermo scientific). Gene expression was quantified relative to the housekeeping gene β-2 microglobulin (B2M) according to the comparative ΔΔCt method.

Chromatin Immunoprecipitation (ChIP)

Approximately 5 x 10^7 cells (after 5 days of doxycycline discontinuation, where appropriate) were seeded on 150 mm dish. After 2 days, cells were washed and fixed in 1 % formaldehyde in serum-free DMEM for 10 min. Cross-linking reaction was stopped by adding glycine (final concentration 125 mM) for 5 min. Media was completely aspirated and cells were washed 4 times with ice cold PBS. Cells were then harvested in 5 ml of ChIP cell lysis buffer (10 mM Tris-HCl pH 8.0, 10 mM NaCl, 0.20 % Igepal CA-630, 10 mM NaBu, 50 μg/ml PMSF and 1 μg/ml Leupeptin) and incubated for 10 min on ice. Cells were then centrifuged at 2,500 rpm for 5 min at 4 °C and nuclei was resuspended and incubated in 1.2 ml of ChIP nuclei lysis buffer (NLB: 50 mM Tris-HCl pH 8.0, 10 mM EDTA, 1 % SDS, 10 mM NaBu, 50 μg/ml PMSF and 1 μg/ml Leupeptin) for 10 min on ice. 0.72 ml of IP dilution buffer (IPDB: 20 mM Tris-HCl, 150 mM NaCl, 2 mM EDTA, 1 % Triton X-100, 0.01% SDS, 10 mM NaBu, 50 μg/ml PMSF and 1 μg/ml Leupeptin) and samples were sonicated using the Bioruptor sonicator (high setting, 30s on-30s off) for 30 min (replaced ice every 10 min). 4.1 ml of IPDB was added and chromatin was precleared by 20 μl of normal mouse IgG (Santa Cruz Biotechnology) and 50 μl of Dynabeads protein G (Life technologies) for 4 hours on a rotating wheel at 4 °C. Modified IPDB (IPDBmod) was made by combining 1:4 NLB:IPDM. Supernatant was transferred to new Eppendorf tubes and set up in necessary conditions for ChIP with p53 and MDM2. Samples were incubated on a rotating wheel overnight at 4 °C.

ChIP Target conditions

p53: 0.675 ml chromatin + 0.675 ml IPDBmod + 7.5 µg p53 antibody (DO-1)

MDM2: 0.675 ml chromatin + 0.675 ml IPDBmod + 7.5 µg MDM2 antibody (Ab-1)

Negative control: 0.675 ml chromatin + 0.675 ml IPDBmod + 7.5 µg IgG

50 µl of Dynabeads protein G was added to the samples and they were incubated for 3 hours on a rotating wheel overnight at 4 °C. Beads were washed twice with IP wash buffer 1 (20 mM Tris-HCl pH8.0, 50 mM NaCl, 2 mM EDTA, 1 % Triton X-100 and 0.001 % SDS), once with IP wash buffer 2 (10 mM Tris-HCl pH8.0, 250 mM LiCl, 1 mM EDTA, 1 % Igepal CA-630 and 1% Deoxycholate), then twice with TE buffer pH8.0. ChIP materials were eluted in 300 µl of ChIP elution buffer (100 mM $NaHCO_3$, 1% SDS, 20 µg RNase and 40 µg Proteinase K) on a Thermomixer heat block (Eppendorf) at 900 rpm overnight for 65 °C. Input samples were similarly processed.

Following this, 200 µl of samples were transferred to fresh Eppendorf tubes and 200 µl of TE buffer. 400 µl of phenol-chloroform-isoamylalcohol (PCI) was added to the samples and they were transferred to the phase-lock tubes (5 Prime) for DNA isolation. Samples were spun at 14,000 r.c.f. for 5 minutes at RT and upper phase was transferred to Eppendorf tubes. 16 µl of 5 M NaCl and 8 µl of glycogen (5 mg/ml) was added and vortexed. 1 ml of ice cold 100 % ethanol was then added to the samples, voetexed and stored at -80 °C for 30 min. Following this, samples were spun at 16,100 r.c.f. for 15 min at 4 °C, and the supernatant was discarded. Pellets were washed with 1 ml ice cold 80 % ethanol and spun at 16,100 r.c.f. for 10 min at 4 °C. The supernatant was discarded and pellets were dried at RT then DNA was eluted in 50 µl 10 mM Tris-HCl and heated on a Thermomixer heat block (Eppendorf) for 10 min at 50 °C in order to dissolve the pellet. Samples were then analyzed via qPCR as

described with a modified PCR programme (20 sec at 95 °C hot start, 45 cycles of 3 sec denaturing at 95 °C, 30 sec annealing-elongation at 60 °C). Primers used are provided in **Supplementary Table 5**. Values were calculated as % input.

Cell growth assay and cell staining

Cells were plated in 24-well plates (after 5 days of doxycycline discontinuation where appropriate). After trypsinization, the number of viable cells was counted using CASY cell counter.

For cell staining, cells were fixed with ice-cold 100 % methanol and stained with 0.04 % SRB (Sulforhodamine B) in 1 % acetic acid. SRB intensity was quantified by ImageJ software.

Statistical analysis and reproducibility

Experimental data are expressed as mean ± S.D. unless otherwise indicted. Statistical differences were analyzed by one- or two-way analysis of variance (ANOVA) followed by Tukey's post-hoc test (two-tailed), as appropriate. F statistics and degrees of freedom for all ANOVAs were reported in **Supplementary Table 3**. All statistical analyses were performed with Prism (GraphPad Software). Statistical significance was defined as $p<0.05$. Each experiment was repeated independently at least three times and sample sizes and number of repeats are defined in each figure legend.

Methods-only References

62. Kabsch, W. Xds. *Acta Crystallogr D Biol Crystallogr* **66**, 125-132 (2010).
63. Collaborative Computational Project, N. "The CCP4 Suite: Programs for Protein Crystallography". *Acta Cryst.* **D50**, 760-763 (1994).

64. Storoni, L.C., McCoy, A.J. & Read, R.J. Likelihood-enhanced fast rotation functions. *Acta Crystallogr D Biol Crystallogr* **60**, 432-438 (2004).
65. Emsley, P. & Cowtan, K. Coot: model-building tools for molecular graphics. *Acta Crystallogr D Biol Crystallogr* **60**, 2126-2132 (2004).
66. Adams, P.D. *et al.* PHENIX: building new software for automated crystallographic structure determination. *Acta Crystallogr D Biol Crystallogr* **58**, 1948-1954 (2002).

Supplementary Table 1 Dissociation constants (K_d) for interactions between MDM2 variants and UbcH5B–Ub

Immobilized Protein	Analyte	K_d (μM)
MDM2 398-C	UbcH5B–Ub + UbΔGG	1.2 ± 0.2
MDM2 398-C I440E	UbcH5B–Ub + UbΔGG	N.M.
MDM2 398-C I440A	UbcH5B–Ub + UbΔGG	N.M.
MDM2 398-C I440D	UbcH5B–Ub + UbΔGG	N.M.
MDM2 398-C I440Y	UbcH5B–Ub + UbΔGG	71 ± 2
MDM2 398-C I440R	UbcH5B–Ub + UbΔGG	N.M.
MDM2 398-C I440K	UbcH5B–Ub + UbΔGG	N.M.
MDM2 398-C R479A	UbcH5B–Ub + UbΔGG	32 ± 1
MDM2 398-C R479P	UbcH5B–Ub + UbΔGG	N.M.
MDM2 398-C R479I	UbcH5B–Ub + UbΔGG	7 ± 1
MDM2 398-C R479F	UbcH5B–Ub + UbΔGG	41 ± 2
MDM2 398-C R479K	UbcH5B–Ub + UbΔGG	22 ± 2
MDM2 398-C R479G	UbcH5B–Ub + UbΔGG	52 ± 2

s.e.m. are indicated. N.M. indicates no measurable binding. Representative sensorgrams and binding curves are shown in **Supplementary Fig. 3a**.

Supplementary Table 2 Summary of MDM2 mutants in this study

MDM2	wild type	C464A	I440K I440E	R479P
Mutation (Structural estimation)	N/A	Disrupts RING domain co-ordination	Does not interact with E2–Ub complex (Disrupts hydrophobic interaction)	Does not interact with E2–Ub complex (Disrupts hydrogen bonds)
Interaction with E2–Ub complex	+++	Not tested	-	-
p53 binding	+++	++	+++	+++
Dimerization with MDMX	+++	-	+++	+++
Ubiquitination of p53	+++	-	-	-
Inhibition of p53 activity	+++	+	+++	+++
Localization on p21 promoter (via p53)	+++	+	+++	+++
Cell growth	+++	+	+++	+++
p53 activation after stress	Slow	N/A	Fast	Fast
Reactivation (Ubiquitination of p53)	N/A	-	When dimerized with appropriate binding partner*	When dimerized with appropriate binding partner*

*Binding partner including MDMX K478R

Supplementary Table 3 ANOVA and the F-statistics

Figures	**ANOVA**	**F(DFn, DFd) value**
6b	One way	F(5, 12) = 21.96 (p53/Actin) F(5, 12) = 131.9 (p21/Actin)
6c	Two way	F(5, 15) = 2.915 (ChIP:p53) F(5, 15) = 8.691 (ChIP:MDM2)
6d	One way	F(5, 12) = 17.04
6e	Two way	F(5, 60) = 41.74 (No Doxy, main effect of mutants)
7a	Two way	F(15, 36) = 5.719 (*cdkn1a(p21)*) F(15, 36) = 2.754 (*tigar*) F(15, 36) = 4.232 (*fas*)
7e	One way	F(5, 24) = 50.50 (ActD 0h treatment) F(5, 24) = 35.76 (ActD 24h treatment) F(5, 24) = 14.39 (ActD 72h treatment) F(5, 24) = 30.38 (ActD 120h treatment)
Supplementary 5	One way	F(4, 10) = 13.10 (*cdkn1a(p21)*) F(4, 10) = 16.80 (*tigar*) F(4, 10) = 7.144 (*fas*) F(4, 10) = 12.48 (*puma*) F(4, 10) = 16.16 (*phlda3*) F(4, 10) = 12.11 (*pig3*) F(4, 10) = 11.16 (*sestrin2*) F(4, 10) = 25.14 (*gadd45α*)

DFn = degrees of freedom numerator
DFd = degrees of freedom denominator

Supplementary Table 4 Plasmids used in this study

Expression				
Encode	Plasmid	Tag	Assays	Reference
p53	pCD6	N/A	Ubiquitination assay Co-IP	[1]
MDM2	pCMV	N/A	Ubiquitination assay Co-IP Immunofluorescence	[2]
MDMX	pcDNA3.1	Myc	Ubiquitination assay Co-IP	[3]
MDMX	pEGFP-C1	GFP	Immunofluorescence	[4]
MDM2/MDMX chimera (1-421: MDM2, 422-490: MDMX)	pCMV	FLAG	Ubiquitination assay Co-IP	[5]
Ubiquitin	pDG268	His GFP	Ubiquitination assay	[6]
mCherry	pmCherry-C1	N/A	Ubiquitination assay Co-IP	[7]
$MDM2^R$ and $MDMX^R$	RSF_Duet	His on ($MDM2^R$)	*In vitro* assay	Current manuscript
$MDM2^R$	pGEX4T1	GST	*In vitro* assay	Current manuscript
$MDMX^R$	pGEX4T1	GST	*In vitro* assay	Current manuscript
$MDM2^R$	RSF_Duet	His	*In vitro* assay	Current manuscript
$MDMX^R$	RSF_Duet	His	*In vitro* assay	Current manuscript
MDM2 398-C	pGEX4T1	GST	*In vitro* assay	Current manuscript
UbcH5B	RSF_Duet	N/A	*In vitro* assay	[8]
Ub	RSF_Duet	His	*In vitro* assay	[8]

Point mutation(s) are based on these plasmids

Knock down or knock out		
Function	Plasmid	Target sequences
Tetracycline inducible p53 knockdown (shRNA)	Tet-pLKO-puro	GAC TCC AGT GGT AAT CTA C
CRISPR/Cas9 MDM2 knock-out (Guide A)	pX335-U6-Chimeric_BB-CBh-hSpCas9n(D10A)	ATC GTT TAG TCA TAA TAT AC <u>TGG</u> (PAM)
CRISPR/Cas9 MDM2 knock-out (Guide B)	pX335-U6-Chimeric_BB-CBh-hSpCas9n(D10A)	TAT TGT TCA AAT GAT CTT CT <u>AGG</u> (PAM)

Tet-pLKO-puro[9] was a gift from Dmitri Wiederschain (Addgene plasmid # 21915)
pX335-U6-Chimeric_BB-CBh-hSpCas9n(D10A)[10] was a gift from Feng Zhang (Addgene plasmid # 42335)

References

1. Chen, J., Lin, J. & Levine, A.J. Regulation of transcription functions of the p53 tumor suppressor by the mdm-2 oncogene. *Mol Med* **1**, 142-152 (1995).
2. Kawai, H., Wiederschain, D. & Yuan, Z.M. Critical contribution of the MDM2 acidic domain to p53 ubiquitination. *Mol Cell Biol* **23**, 4939-4947 (2003).
3. Weber, H.O. *et al.* HDM2 phosphorylation by MAPKAP kinase 2. *Oncogene* **24**, 1965-1972 (2005).
4. Uldrijan, S., Pannekoek, W.J. & Vousden, K.H. An essential function of the extreme C-terminus of MDM2 can be provided by MDMX. *EMBO J* **26**, 102-112 (2007).
5. Sharp, D.A., Kratowicz, S.A., Sank, M.J. & George, D.L. Stabilization of the MDM2 oncoprotein by interaction with the structurally related MDMX protein. *J Biol Chem* **274**, 38189-38196 (1999).
6. Tsirigotis, M., Zhang, M., Chiu, R.K., Wouters, B.G. & Gray, D.A. Sensitivity of mammalian cells expressing mutant ubiquitin to protein-damaging agents. *J Biol Chem* **276**, 46073-46078 (2001).
7. Werner, H., Karnieli, E., Rauscher, F.J. & LeRoith, D. Wild-type and mutant p53 differentially regulate transcription of the insulin-like growth factor I receptor gene. *Proc Natl Acad Sci U S A* **93**, 8318-8323 (1996).
8. Dou, H., Buetow, L., Sibbet, G.J., Cameron, K. & Huang, D.T. BIRC7-E2 ubiquitin conjugate structure reveals the mechanism of ubiquitin transfer by a RING dimer. *Nat Struct Mol Biol* **19**, 876-883 (2012).
9. Wiederschain, D. *et al.* Single-vector inducible lentiviral RNAi system for oncology target validation. *Cell Cycle* **8**, 498-504 (2009).
10. Cong, L. *et al.* Multiplex genome engineering using CRISPR/Cas systems. *Science* **339**, 819-823 (2013).

Supplementary Table 5 Primers used for qPCR or ChIP (5'-3')

B2M	for	GTG CTC GCG CTA CTC TCT C
	rev	GTC AAC TTC AAT GTC GGA T
CDKN1A (p21)	for	TGG GAG CGG ATA GAC ACA TC
	rev	GGC TCT CTG CTT GTC ATC CTT
TIGAR	for	CGC GTG GAG AAA CAA GAT TT
	rev	CCG TAT TTC CTT TCC CGA AG
FAS	for	GTA CGG AGT TGG GGA AGC TC
	rev	AGG GCT TAT GGC AGA ATT GG
PUMA	for	GAA TCC ACG GCT TTG GAA AA
	rev	TGG CCA CAC TCA CCA CAA AT
PHLDA3	for	GAC CCT CGT GTC CTA AAC CA
	rev	CTC GTC CAT TCC TTC AGC TC
PIG3	for	TCT CTG AAG CAA CGC TGA AAT TC
	rev	ACG TTC TTC TCC CAG TAG GAT CC
Sestrin2	for	ACT CTG GGG GCT TTG AGT CT
	rev	GTC TTC CAC AAA GCA CAG CA
GADD45 α	for	CAG AAG ACC GAA AGG ATG GA
	rev	ATC TCT GTC GTC GTC CTC GT
GADD45 β	for	CGC TGG AAG AGC TCG TGG CG
	rev	ACC ACG CTG TCT GGG TCC ACA T
p21 -2350 bp	for	CTG GAC TGG GCA CTC TTG TC
(promoter)	rev	CCC CTT CCT CAC CTG AAA AC
p21 +50 bp	for	GGC ACT CAG AGG AGG TGA GA
(non specific)	rev	ACC CGC GCA CTT AGA GAC AC

Supplementary Table 6 Antibodies used in cell-based experiments

Primary Antibody	Description	Supplier	Dilution or amount
p53	mouse monoclonal (DO-1)	Santa Cruz Biotechnology	1:1000 (WB) 2 μg (IP) 7.5 μg (ChIP)
p53	rabbit polyclonal (FL-393)	Santa Cruz Biotechnology	1:1000 (WB)
MDM2	mouse monoclonal (Ab-1)	Calbiochem	1:1000 (WB) 2 μg (IP) 1:100 (IF) 7.5 μg (ChIP)
MDMX	rabbit polyclonal (A300-287A)	Bethyl Laboratories	1:1000 (WB) 2 μg (IP)
MDMX	mouse monoclonal (8C6)	EMD Millipore	1:1000 (WB)
PIG3	rabbit polyclonal (PC268)	Calbiochem	1:1000 (WB)
TIGAR	mouse monoclonal (F-5)	Santa Cruz Biotechnology	1:1000 (WB)
BAX	mouse monoclonal (D2D)	Santa Cruz Biotechnology	1:1000 (WB)
phospho-p53 (S15)	rabbit polyclonal (9284)	Cell Signaling Technology	1:1000 (WB)
phospho-p53 (S20)	rabbit polyclonal (9287)	Cell Signaling Technology	1:1000 (WB)
Actin	rabbit or goat polyclonal (I-19)	Santa Cruz Biotechnology	1:1000 (WB)
α Tubulin	mouse monoclonal (DM1A)	Santa Cruz Biotechnology	1:1000 (WB)
mCherry	goat polyclonal (AB0040)	Acris Antibodies	1:2500 (WB)
Secondary antibody			
Alexa568-conjugated donkey anti mouse		Life Technologies	1:200 (IF)
IRDye 680LT-conjugated secondary antibody		LI-COR	1:10000 (WB)
IRDye 800CW- conjugated secondary antibody		LI-COR	1:10000 (WB)

WB = Western blotting
IP = Immunoprecipitation
IF = Immunofluorescence
ChIP = Chromatin immunoprecipitation

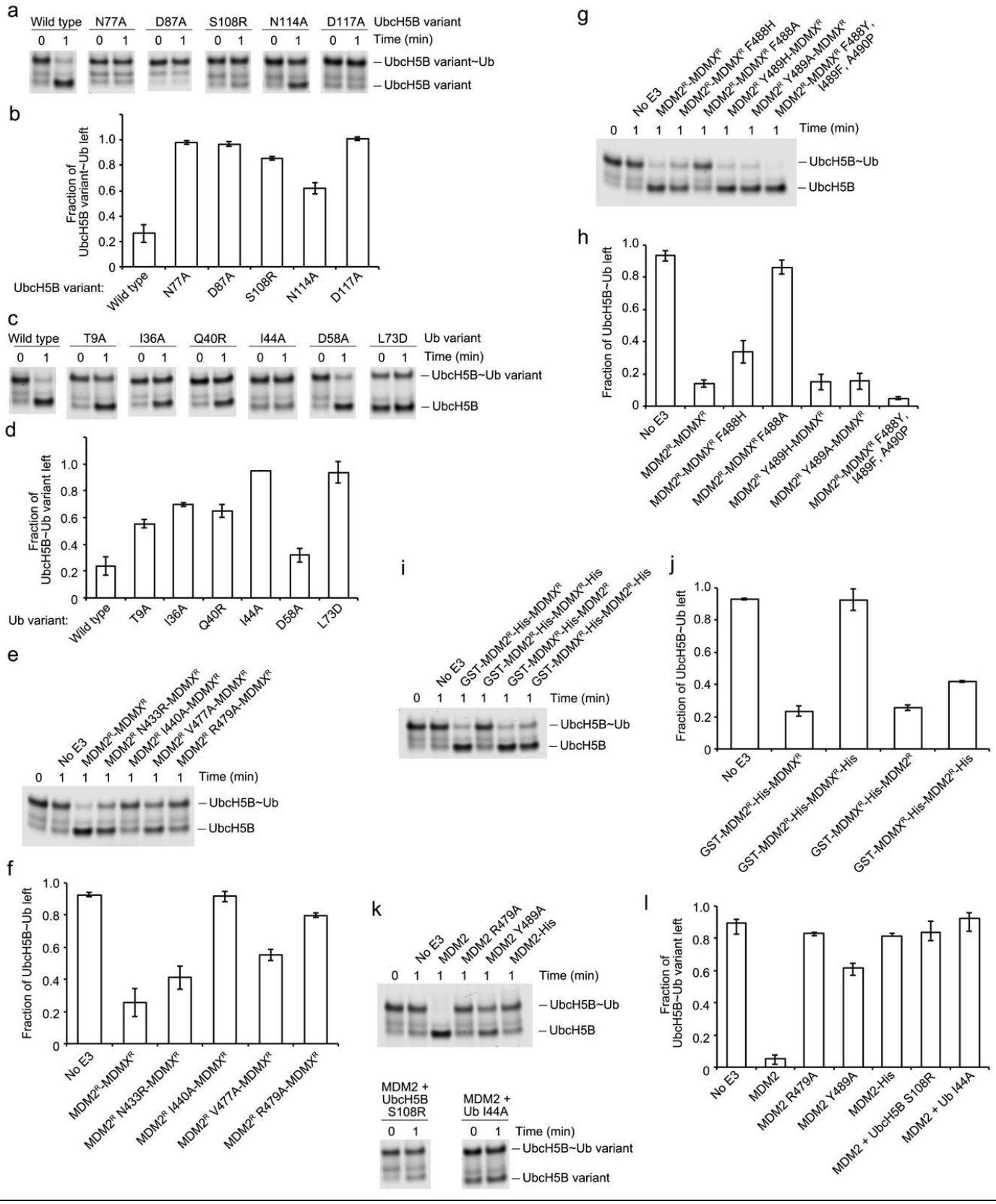
a
Wild type
N77A
D87A
S108R
N114A
D117A
UbcH5B variant
0 1
Time (min)
– UbcH5B variant~Ub
– UbcH5B variant
b
Fraction of UbcH5B variant~Ub left
1.0
0.8
0.6
0.4
0.2
0
UbcH5B variant:
Wild type
N77A
D87A
S108R
N114A
D117A
c
Wild type
T9A
I36A
Q40R
I44A
D58A
L73D
Ub variant
Time (min)
– UbcH5B~Ub variant
– UbcH5B
d
Fraction of UbcH5B~Ub variant left
Ub variant:
Wild type
T9A
I36A
Q40R
I44A
D58A
L73D
e
No E3
MDM2R-MDMXR
MDM2R N433R-MDMXR
MDM2R I440A-MDMXR
MDM2R V477A-MDMXR
MDM2R R479A-MDMXR
0 1 1 1 1 1 1
Time (min)
– UbcH5B~Ub
– UbcH5B
f
Fraction of UbcH5B~Ub left
No E3
MDM2R-MDMXR
MDM2R N433R-MDMXR
MDM2R I440A-MDMXR
MDM2R V477A-MDMXR
MDM2R R479A-MDMXR
g
No E3
MDM2R-MDMXR
MDM2R-MDMXR F488H
MDM2R-MDMXR F488A
MDM2R Y489H-MDMXR
MDM2R Y489A-MDMXR
MDM2R-MDMXR F488Y, I489F, A490P
0 1 1 1 1 1 1 1
Time (min)
– UbcH5B~Ub
– UbcH5B
h
Fraction of UbcH5B~Ub left
No E3
MDM2R-MDMXR
MDM2R-MDMXR F488H
MDM2R-MDMXR F488A
MDM2R Y489H-MDMXR
MDM2R Y489A-MDMXR
MDM2R-MDMXR F488Y, I489F, A490P
i
No E3
GST-MDM2R-His-MDMXR
GST-MDM2R-His-MDMXR-His
GST-MDMXR-His-MDM2R
GST-MDMXR-His-MDM2R-His
0 1 1 1 1 1
Time (min)
– UbcH5B~Ub
– UbcH5B
j
Fraction of UbcH5B~Ub left
No E3
GST-MDM2R-His-MDMXR
GST-MDM2R-His-MDMXR-His
GST-MDMXR-His-MDM2R
GST-MDMXR-His-MDM2R-His
k
No E3
MDM2
MDM2 R479A
MDM2 Y489A
MDM2-His
0 1 1 1 1 1
Time (min)
– UbcH5B~Ub
– UbcH5B
MDM2 + UbcH5B S108R
0 1
MDM2 + Ub I44A
0 1
Time (min)
– UbcH5B~Ub variant
– UbcH5B variant
l
Fraction of UbcH5B~Ub variant left
No E3
MDM2
MDM2 R479A
MDM2 Y489A
MDM2-His
MDM2 + UbcH5B S108R
MDM2 + Ub I44A

Supplementary Figure 1

UbcH5B~Ub discharge catalyzed by MDM2 and MDM2-MDMX

(**a**) A representative nonreduced SDS-PAGE showing the effects of UbcH5B mutations in discharging UbcH5B variant~Ub to L-lysine in 1 min catalyzed by $MDM2^{R}$-$MDMX^{R}$. (**b**) A bar graph showing the fraction of UbcH5B variant~Ub left in **a**. (**c**) A representative nonreduced SDS-PAGE showing the effects of Ub mutations in discharging UbcH5B~Ub variant to L-lysine in 1 min catalyzed by $MDM2^{R}$-$MDMX^{R}$. (**d**) A bar graph showing the fraction of UbcH5B variant~Ub left in **c**. (**e**) A representative nonreduced SDS-PAGE showing the effects of MDM2 mutations in discharging UbcH5B~Ub to L-lysine in 1 min catalyzed by $MDM2^{R}$-$MDMX^{R}$ variants. (**f**) A bar graph showing the fraction of UbcH5B~Ub left in **e**. (**g**) A representative nonreduced SDS-PAGE showing the discharge of UbcH5B~Ub to L-lysine in 1 min catalyzed by $MDM2^{R}$-$MDMX^{R}$ variants. (**h**) A bar graph showing the fraction of UbcH5B~Ub left in **g**. (**i**) A representative nonreduced SDS-PAGE showing the discharge of UbcH5B~Ub to L-lysine in 1 min catalyzed by $MDM2^{R}$-$MDMX^{R}$ variants. (**j**) A bar graph showing the fraction of UbcH5B~Ub left in **i**. (**k**) A representative nonreduced SDS-PAGE showing the discharge of UbcH5B~Ub to L-lysine in 1 min catalyzed by GST-MDM2 variants. (**l**) A bar graph showing the fraction of UbcH5B~Ub left in **k**. Three independent reactions were performed (n=3) and error bars indicate standard deviation.

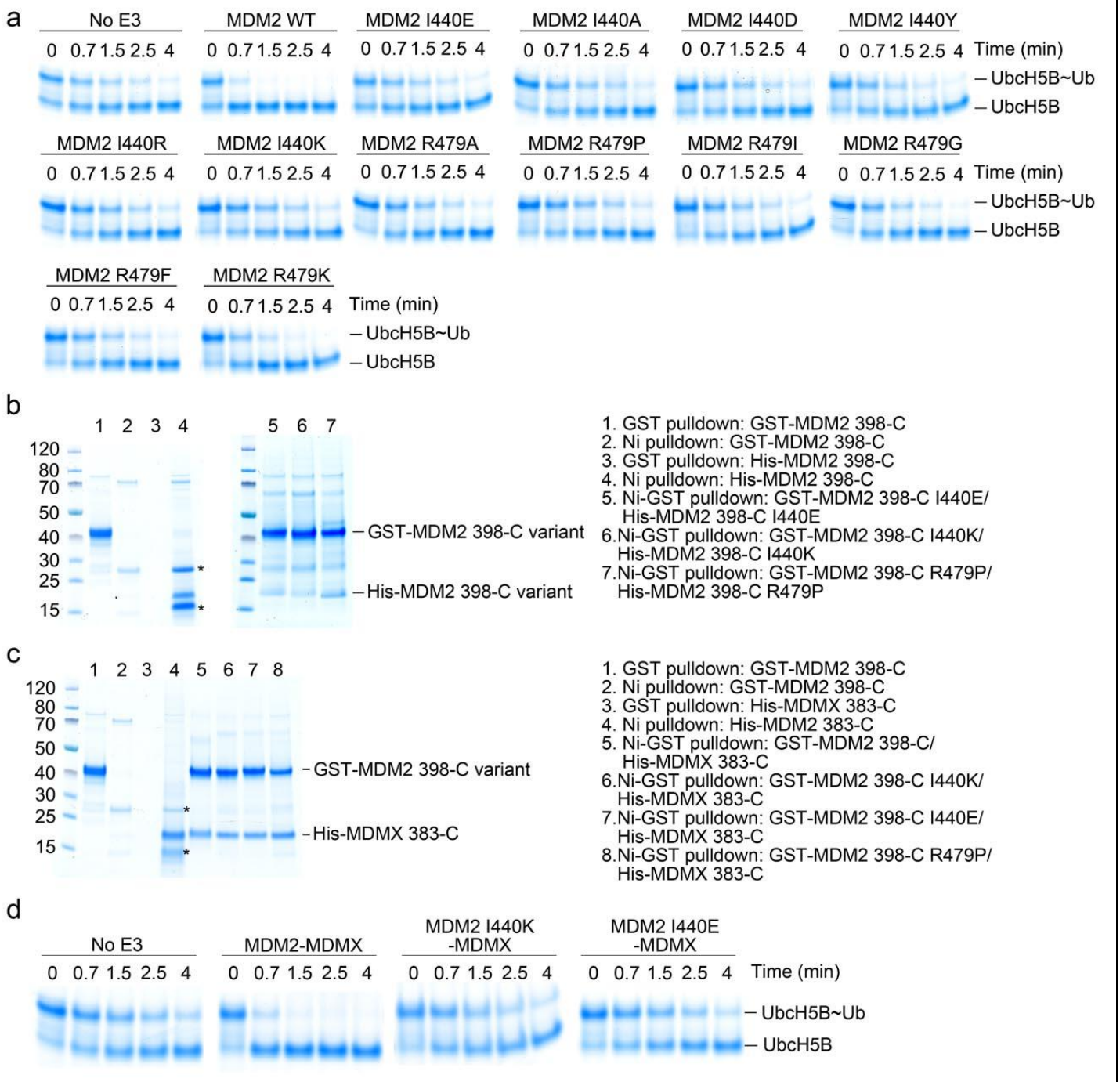

Supplementary Figure 2

Redesigning ligase-dead MDM2 mutants

(**a**) Nonreduced SDS-PAGE showing the discharge of UbcH5B~Ub to L-lysine over time catalyzed by MDM2 I440 and R479 variants. (**b**) SDS-PAGE showing the pull-down experiments of GST-MDM2 I440E, I440K and R479P with His-MDM2 I440E, I440K and R479P, respectively. GST-MDM2 variant and the corresponding His-MDM2 variant were co-expressed in *E. coli* and purified by Ni-NTA affinity followed by glutathione sepharose affinity chromatography. (**c**) SDS-PAGE showing the pull-down experiments of GST-MDM2 variants with His-MDMX. GST-MDM2 variant and His-MDMX were co-expressed in *E. coli* and purified by Ni-NTA affinity followed by glutathione

sepharose affinity chromatography. (**d**) Nonreduced SDS-PAGE showing the discharge of UbcH5B~Ub to L-lysine over time catalyzed by MDM2-MDMX variants. Asterisks indicate contaminants.

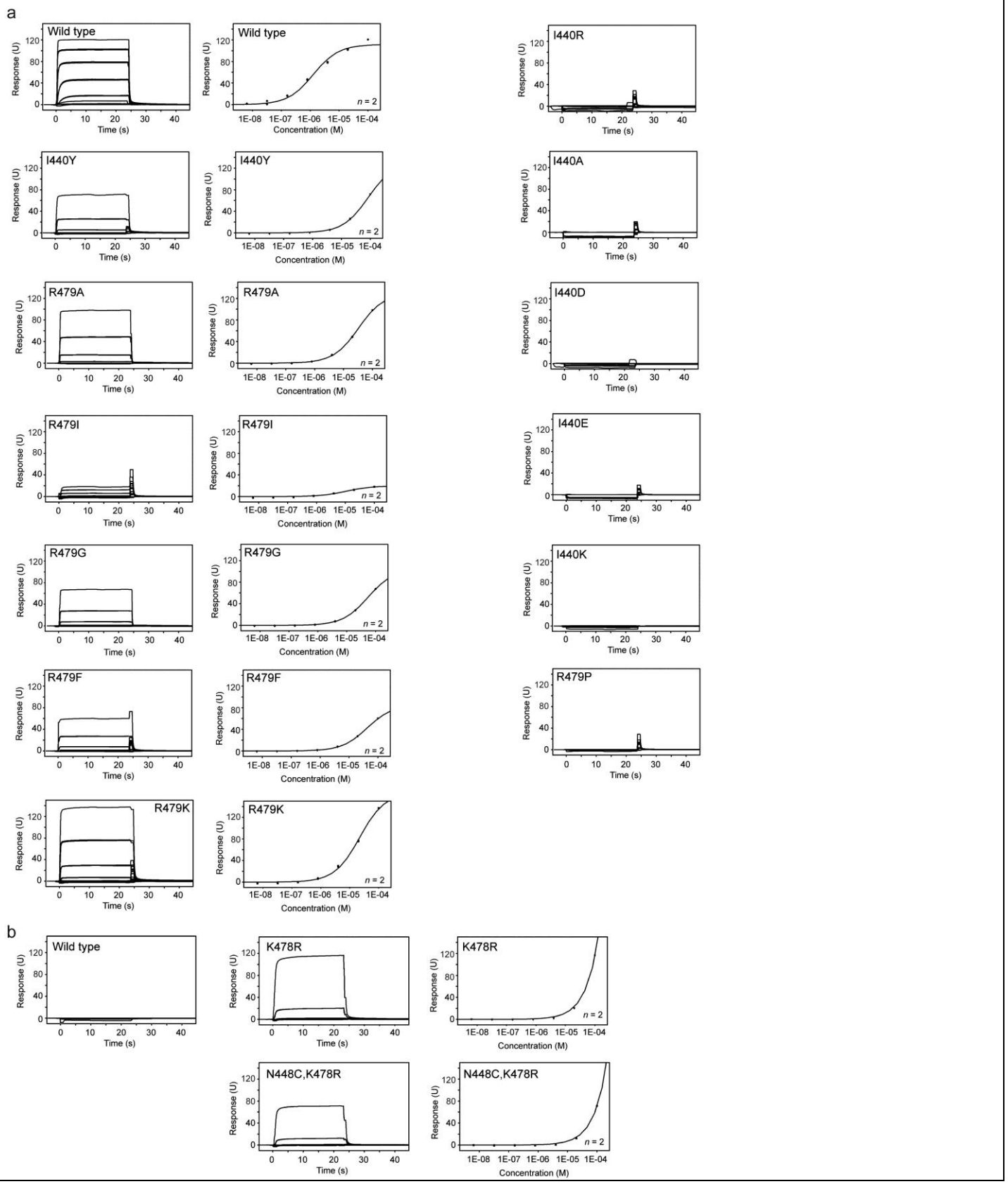
a
Wild type
Wild type
I440R
I440Y
I440Y
I440A
R479A
R479A
I440D
R479I
R479I
I440E
R479G
R479G
I440K
R479F
R479F
R479P
R479K
R479K
Response (U)
Time (s)
Concentration (M)
n = 2
b
Wild type
K478R
K478R
N448C,K478R
N448C,K478R

Supplementary Figure 3

SPR analyses of MDM2 and MDMX variants binding affinities for UbcH5B–Ub

(a) Representative sensorgrams (left) and binding curves (right) for GST-MDM2 398-C variants with UbcH5B–Ub in the presence of UbΔGG are shown. Only sensorgram is shown for GST-MDM2 398-C variants that displayed no measurable UbcH5B–Ub binding in the presence of UbΔGG. **(b)** Representative sensorgrams (left) and binding curves (right) for GST-MDMX^{R} variants with UbcH5B–Ub are shown. Wild type MDMX displayed no UbcH5B–Ub binding up to 100 μM UbcH5B–Ub whereas both K478R and N448C, K478R mutants exhibited UbcH5B–Ub binding. However, K_d could not be estimated due to the weak binding affinity. All experiments in **a** and **b** were performed in duplicates.

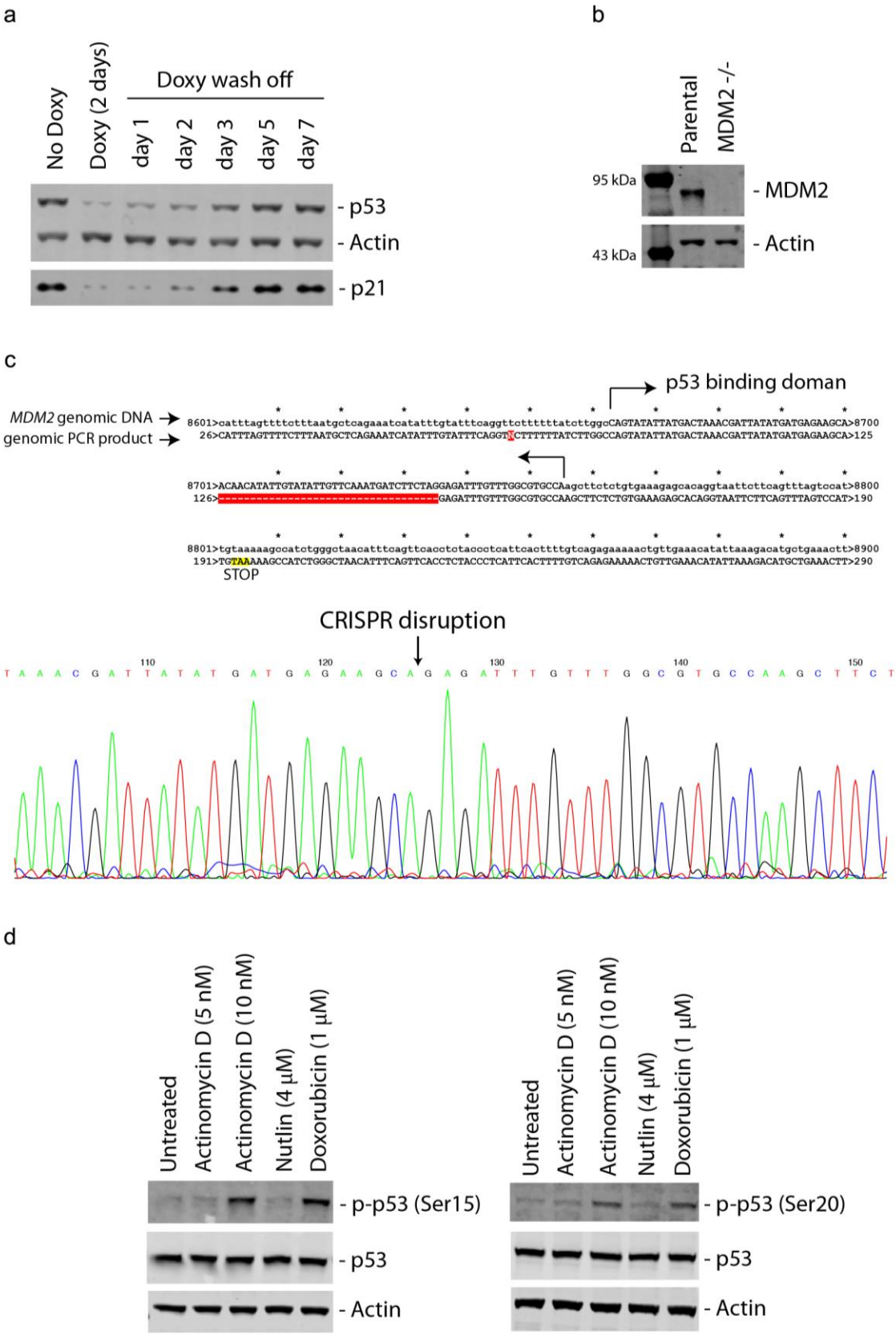
a
No Doxy
Doxy (2 days)
Doxy wash off
day 1
day 2
day 3
day 5
day 7
- p53
- Actin
- p21
b
Parental
MDM2 -/-
95 kDa
- MDM2
43 kDa
- Actin
c
p53 binding doman
MDM2 genomic DNA
genomic PCR product
8601>catttagttttctttaatgctcagaaatcatatttgtatttcaggtTctttttttatcttggccagtatattatgactaaacgattatatgatgagaagca>8700
26>CATTTAGTTTTCTTTAATGCTCAGAAATCATATTTGTATTTCAGGTTCTTTTTTATCTTGGCCAGTATATTATGACTAAACGATTATATGATGAGAAGCA>125
8701>acaacatattgtatattgttcaaatgatcttctaggagatttgtttggcgtgccAagcttctctgtgaaagagcacaggtaattcttcagtttagtccat>8800
126>----------GAGATTTGTTTGGCGTGCCAAGCTTCTCTGTGAAAGAGCACAGGTAATTCTTCAGTTTAGTCCAT>190
8801>tgtaaaaagccatctgggctaacatttcagttcacctctacccctcattcacttttgtcagagaaaaactgttgaaacatattaaagacatgctgaaacct>8900
191>TGTAAAAGCCATCTGGGCTAACATTTCAGTTCACCTCTACCCTCATTCACTTTTGTCAGAGAAAAACTGTTGAAACATATTAAAGACATGCTGAAACTT>290
STOP
CRISPR disruption
110
120
130
140
150
T A A A C G A T T A T A T G A T G A G A A G C A G A G A T T T G T T T G G C G T G C C A A G C T T C T
d
Untreated
Actinomycin D (5 nM)
Actinomycin D (10 nM)
Nutlin (4 μM)
Doxorubicin (1 μM)
- p-p53 (Ser15)
- p53
- Actin
Untreated
Actinomycin D (5 nM)
Actinomycin D (10 nM)
Nutlin (4 μM)
Doxorubicin (1 μM)
- p-p53 (Ser20)
- p53
- Actin

Supplementary Figure 4

Validation of tetracycline inducible p53 knockdown and MDM2 knock-out cells.

U2OS cells were infected with pLKO tet-on shp53. **(a)** Western blot showing that doxycycline treatment causes p53 knock-down in 2 days and this effect can be washed off in 5 days. **(b)** MDM2 was then disrupted by CRISPR. Immunoblotting showing CRISPR disruption (target p53 binding domain) resulted in MDM2 knock-out. **(c)** Genomic PCR followed by sequencing showing that CRISPR disruption (target p53 binding domain) caused MDM2 knock-out. **(d)** MDM2 knock-out cells were treated with indicated drugs for 4 hours and phosphorylated p53 (serine 15 and serine 20) are analyzed by western blot.

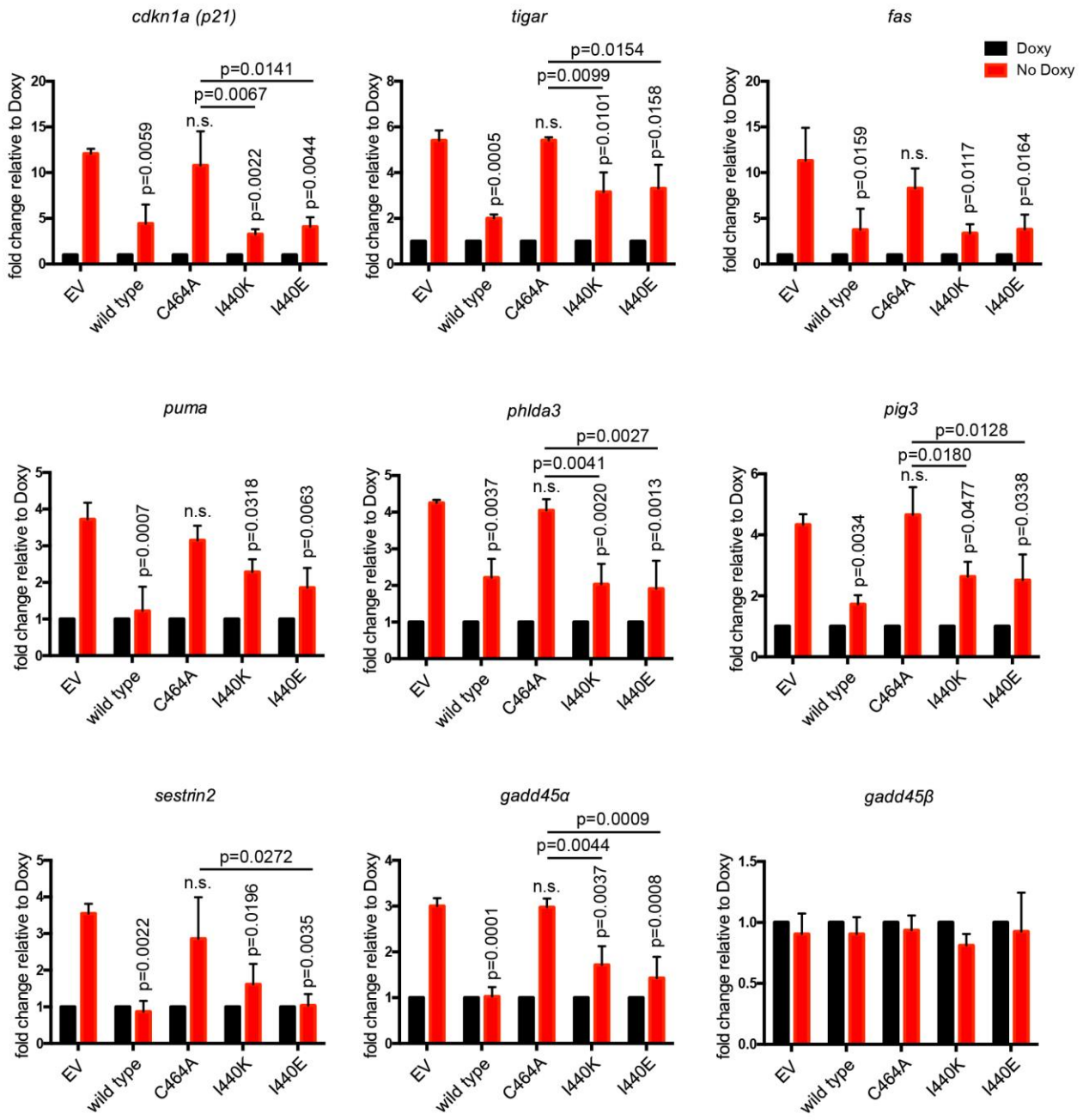

Supplementary Figure 5

MDM2 mutants can limit induction of p53 target genes.

qPCR showing mRNA expression of p53 target genes (gadd45β is not a p53 target gene) is attenuated by MDM2 I440K, I440E but not by C464A. n = 3 independent experiments each. p values: v.s. EV No Doxy (vertical), v.s. C464A No Doxy (horizontal). n.s. indicates non-significant. F-statistics and degrees of freedom of ANOVAs are reported in **Supplementary Table 3**.

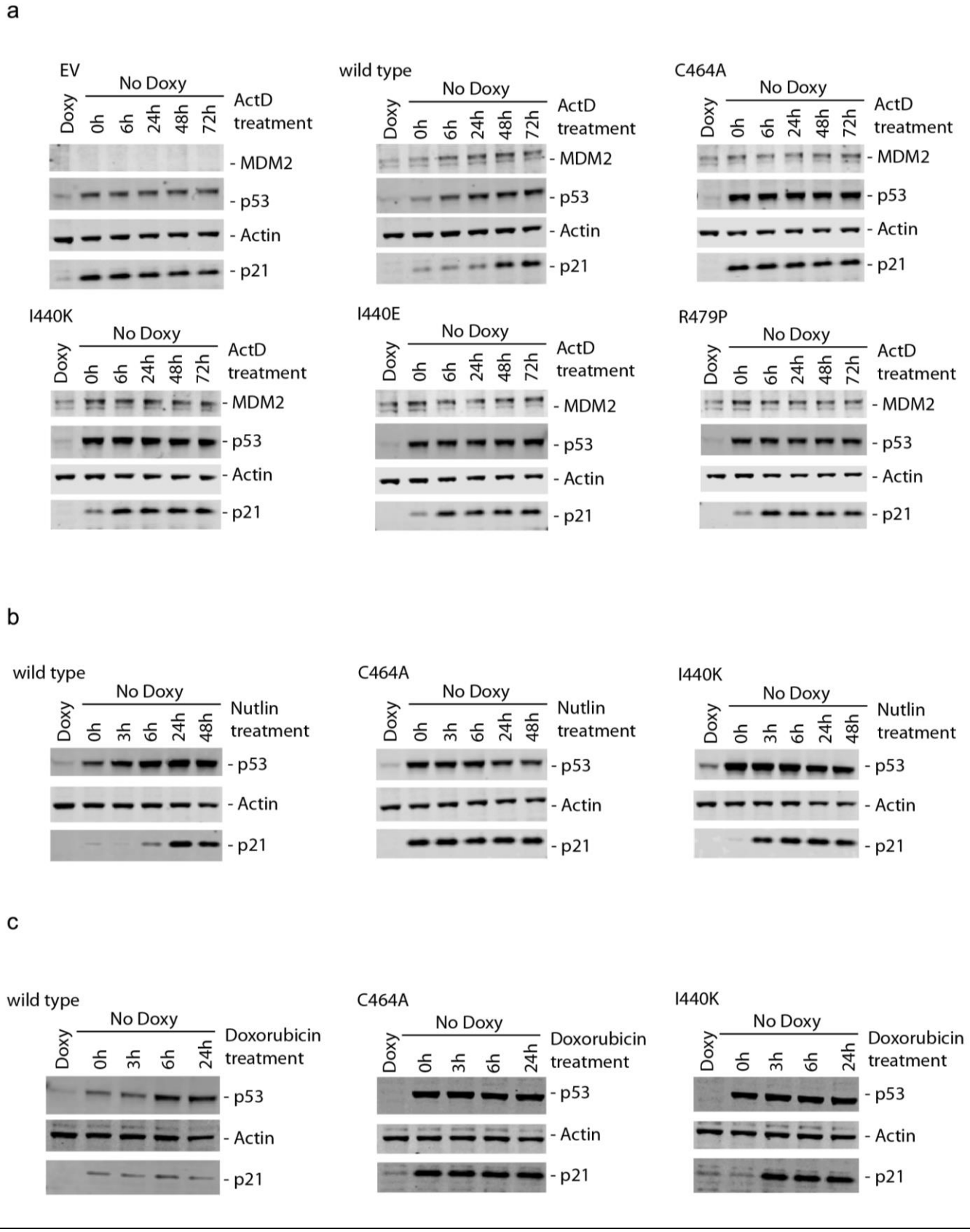
a
EV
No Doxy
Doxy
0h
6h
24h
48h
72h
ActD treatment
- MDM2
- p53
- Actin
- p21
wild type
C464A
I440K
I440E
R479P
b
wild type
No Doxy
Doxy
0h
3h
6h
24h
48h
Nutlin treatment
- p53
- Actin
- p21
C464A
I440K
c
wild type
No Doxy
Doxy
0h
3h
6h
24h
Doxorubicin treatment
- p53
- Actin
- p21
C464A
I440K

Supplementary Figure 6

MDM2 I440 and R479 mutants can rapidly respond to the stress.

(a) Immunoblots showing that following wild type p53 re-expression by removal of Doxycycline (Doxy), p21 is more rapidly induced in cells expressing MDM2 I440 and R479 in response to Actinomycin D treatment compared to cells expressing wild type MDM2 (see **Fig. 5c**). Similar responses in cells treated with 4 μM Nutlin **(b)** and 1 μM Doxorubicin **(c)**.

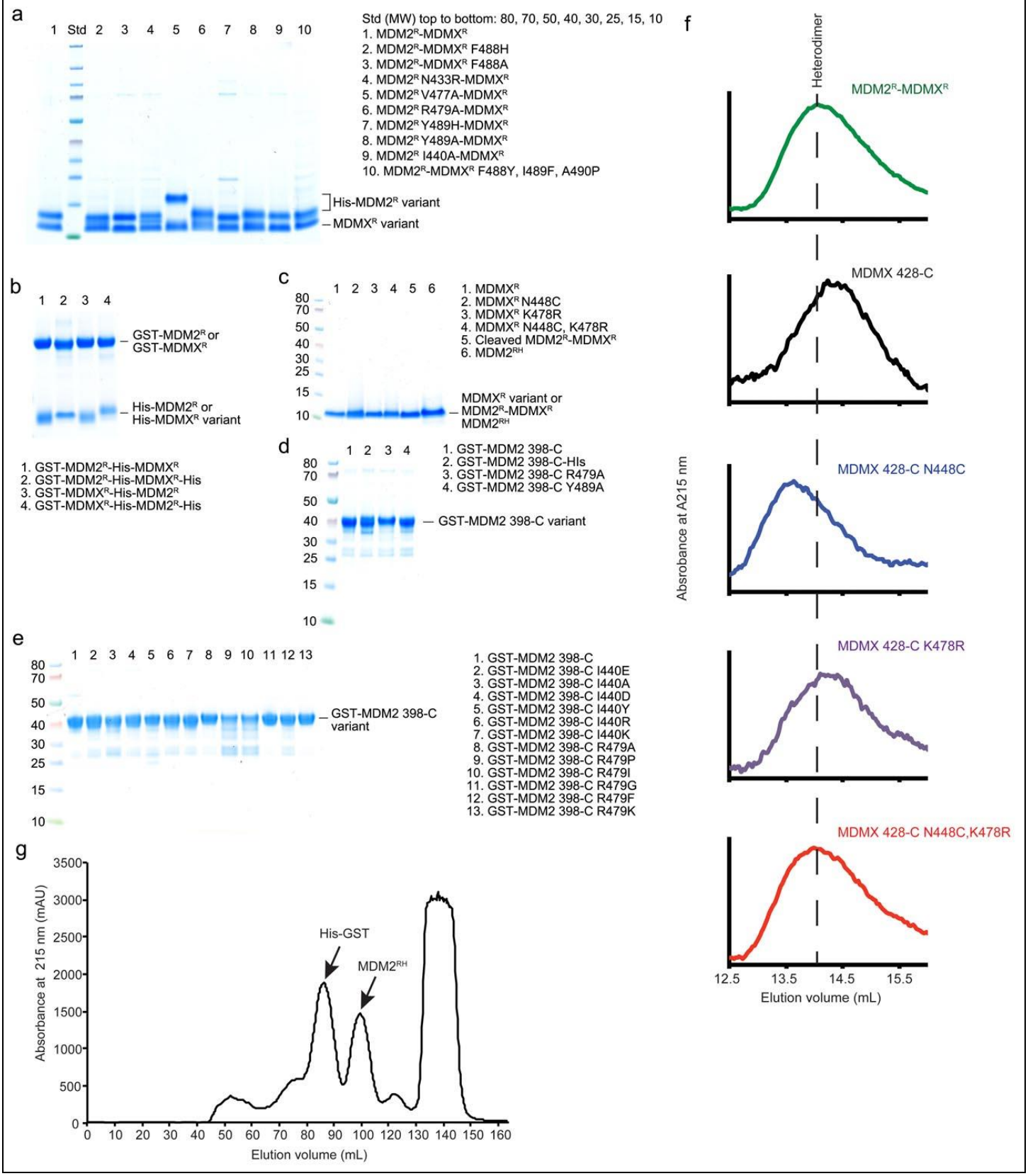
a
1 Std 2 3 4 5 6 7 8 9 10
Std (MW) top to bottom: 80, 70, 50, 40, 30, 25, 15, 10
1. MDM2R-MDMXR
2. MDM2R-MDMXR F488H
3. MDM2R-MDMXR F488A
4. MDM2R N433R-MDMXR
5. MDM2R V477A-MDMXR
6. MDM2R R479A-MDMXR
7. MDM2R Y489H-MDMXR
8. MDM2R Y489A-MDMXR
9. MDM2R I440A-MDMXR
10. MDM2R-MDMXR F488Y, I489F, A490P
His-MDM2R variant
MDMXR variant
b
1 2 3 4
GST-MDM2R or GST-MDMXR
His-MDM2R or His-MDMXR variant
1. GST-MDM2R-His-MDMXR
2. GST-MDM2R-His-MDMXR-His
3. GST-MDMXR-His-MDM2R
4. GST-MDMXR-His-MDM2R-His
c
1 2 3 4 5 6
80 70 50 40 30 25 15 10
1. MDMXR
2. MDMXR N448C
3. MDMXR K478R
4. MDMXR N448C, K478R
5. Cleaved MDM2R-MDMXR
6. MDM2RH
MDMXR variant or MDM2R-MDMXR MDM2RH
d
1 2 3 4
80 70 50 40 30 25 15 10
1. GST-MDM2 398-C
2. GST-MDM2 398-C-HIs
3. GST-MDM2 398-C R479A
4. GST-MDM2 398-C Y489A
GST-MDM2 398-C variant
e
1 2 3 4 5 6 7 8 9 10 11 12 13
80 70 50 40 30 25 15 10
GST-MDM2 398-C variant
1. GST-MDM2 398-C
2. GST-MDM2 398-C I440E
3. GST-MDM2 398-C I440A
4. GST-MDM2 398-C I440D
5. GST-MDM2 398-C I440Y
6. GST-MDM2 398-C I440R
7. GST-MDM2 398-C I440K
8. GST-MDM2 398-C R479A
9. GST-MDM2 398-C R479P
10. GST-MDM2 398-C R479I
11. GST-MDM2 398-C R479G
12. GST-MDM2 398-C R479F
13. GST-MDM2 398-C R479K
f
Heterodimer
MDM2R-MDMXR
MDMX 428-C
MDMX 428-C N448C
MDMX 428-C K478R
MDMX 428-C N448C,K478R
Absrobance at A215 nm
12.5 13.5 14.5 15.5
Elution volume (mL)
g
Absorbance at 215 nm (mAU)
3500 3000 2500 2000 1500 1000 500 0
His-GST
MDM2RH
0 10 20 30 40 50 60 70 80 90 100 120 130 140 150 160
Elution volume (mL)

Supplementary Figure 7

Purified proteins used in the assays and size exclusion chromatography profiles

(**a**) SDS-PAGE showing $MDM2^{R}$-$MDMX^{R}$ variants. (**b**) SDS-PAGE showing GST-$MDM2^{R}$-His-$MDMX^{R}$ and GST-$MDMX^{R}$-His-$MDM2^{R}$ variants. (**c**) SDS-PAGE showing $MDMX^{R}$ variants, $MDM2^{R}$-$MDMX^{R}$ and $MDMX^{RH}$. (**d**) SDS-PAGE showing GST-$MDMX^{R}$ variants. (**e**) SDS-PAGE showing GST-MDM2 398-C variants. (**f**) Superdex 75 10/300 gel filtration chromatography profile of $MDM2^{R}$-$MDMX^{R}$ and $MDMX^{R}$ variants. Full length MDMX has been reported to dimerize with K_d of 1 μM (Bista, M. et al., *Proceedings of the National Academy of Sciences of the United States of America* **110**, 17814-17819, 2013). To assess the dimerization state of $MDMX^{R}$ variant, protein samples (10 μM, 100 μl) were loaded onto superdex 75 10/300. The dotted line indicates the elution volume of $MDM2^{R}$-$MDMX^{R}$ heterodimer. $MDMX^{R}$ variants containing N448C substitution eluted similar or slightly earlier than this line indicating dimer formation, whereas MDMX variants lacking N448C substitution eluted later than this line, presumably exist as monomer. (**g**) HiLoad 26/600 Superdex 200 chromatography profile of $MDM2^{RH}$ purification. His-GST-$MDM2^{R}$ was incubated with TEV protease to release His-GST tag, followed by Ni-NTA pass-back. The cleaved sample was loaded directly onto HiLoad 26/600 Superdex 200. Trace amount of $MDM2^{R}$ was found throughout the elution profile (45-95 ml) with the majority of $MDM2^{R}$ eluted between 95-110 ml consistent with an earlier report showing that $MDM2^{R}$ exists as dimer and aggregate (Poyurovsky, M.V. et al *Embo Journal* **26**, 90-101, 2007). $MDM2^{RH}$ peak (indicated by arrow) eluted after His-GST peak (indicated by arrow; 50 kDa) was assumed as dimer and was pooled and concentrated for activity assay in **Fig. 3d**.

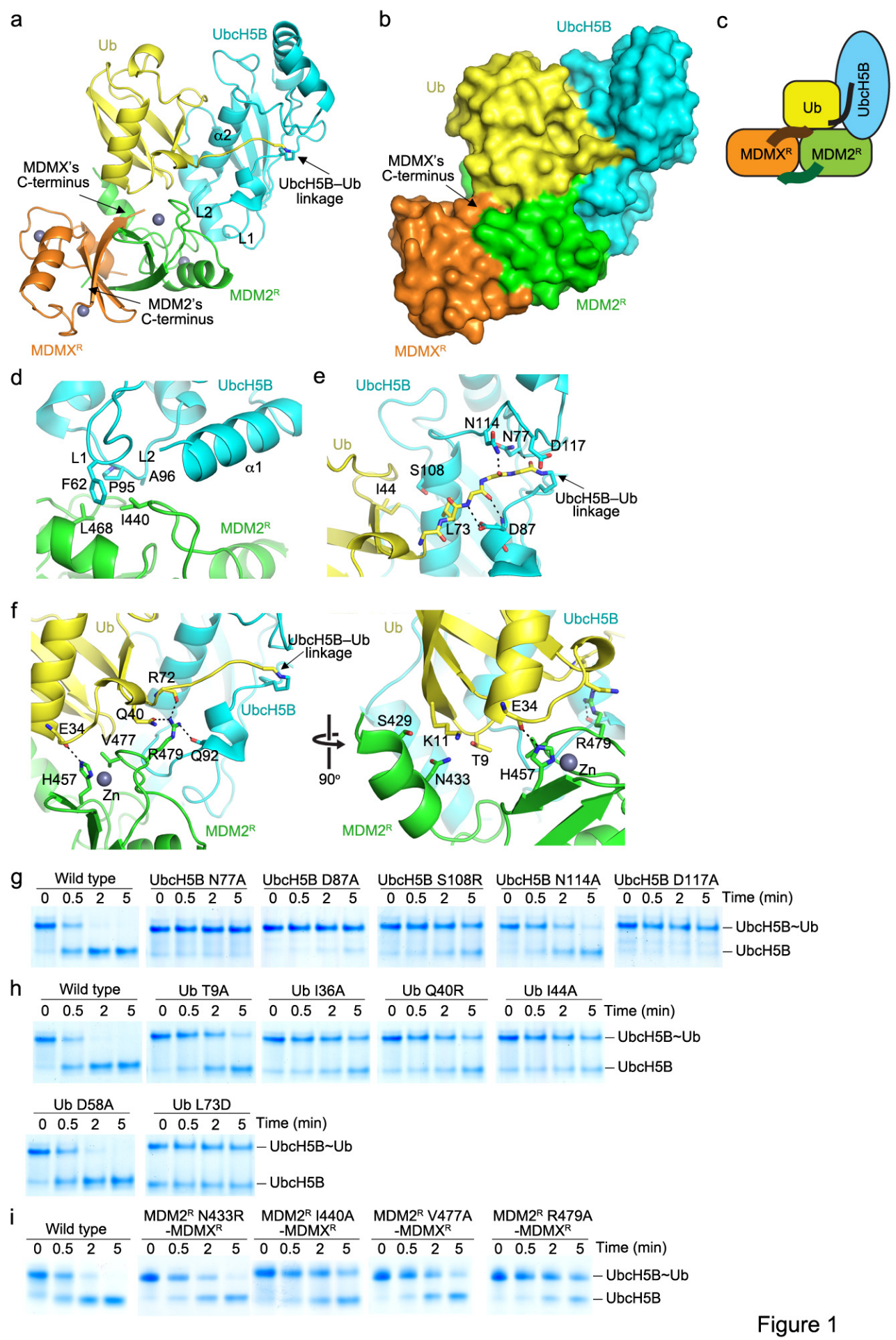
a
Ub
UbcH5B
α2
MDMX's
C-terminus
UbcH5B–Ub
linkage
L2
L1
MDM2's
C-terminus
MDM2R
MDMX R
b
UbcH5B
Ub
MDMX's
C-terminus
MDM2R
MDMX R
c
UbcH5B
Ub
MDMX R
MDM2R
d
UbcH5B
L1
L2
α1
F62
P95
A96
L468
I440
MDM2R
e
UbcH5B
Ub
N114
N77
D117
S108
I44
UbcH5B–Ub
linkage
L73
D87
f
Ub
UbcH5B–Ub
linkage
R72
Q40
UbcH5B
E34
V477
R479
Q92
H457
Zn
MDM2R
90°
Ub
UbcH5B
E34
S429
K11
T9
R479
H457
Zn
N433
MDM2R
g
Wild type
UbcH5B N77A
UbcH5B D87A
UbcH5B S108R
UbcH5B N114A
UbcH5B D117A
0 0.5 2 5
Time (min)
UbcH5B~Ub
UbcH5B
h
Wild type
Ub T9A
Ub I36A
Ub Q40R
Ub I44A
Ub D58A
Ub L73D
0 0.5 2 5
Time (min)
UbcH5B~Ub
UbcH5B
i
Wild type
MDM2R N433R
-MDMX R
MDM2R I440A
-MDMX R
MDM2R V477A
-MDMX R
MDM2R R479A
-MDMX R
0 0.5 2 5
Time (min)
UbcH5B~Ub
UbcH5B

Figure 1

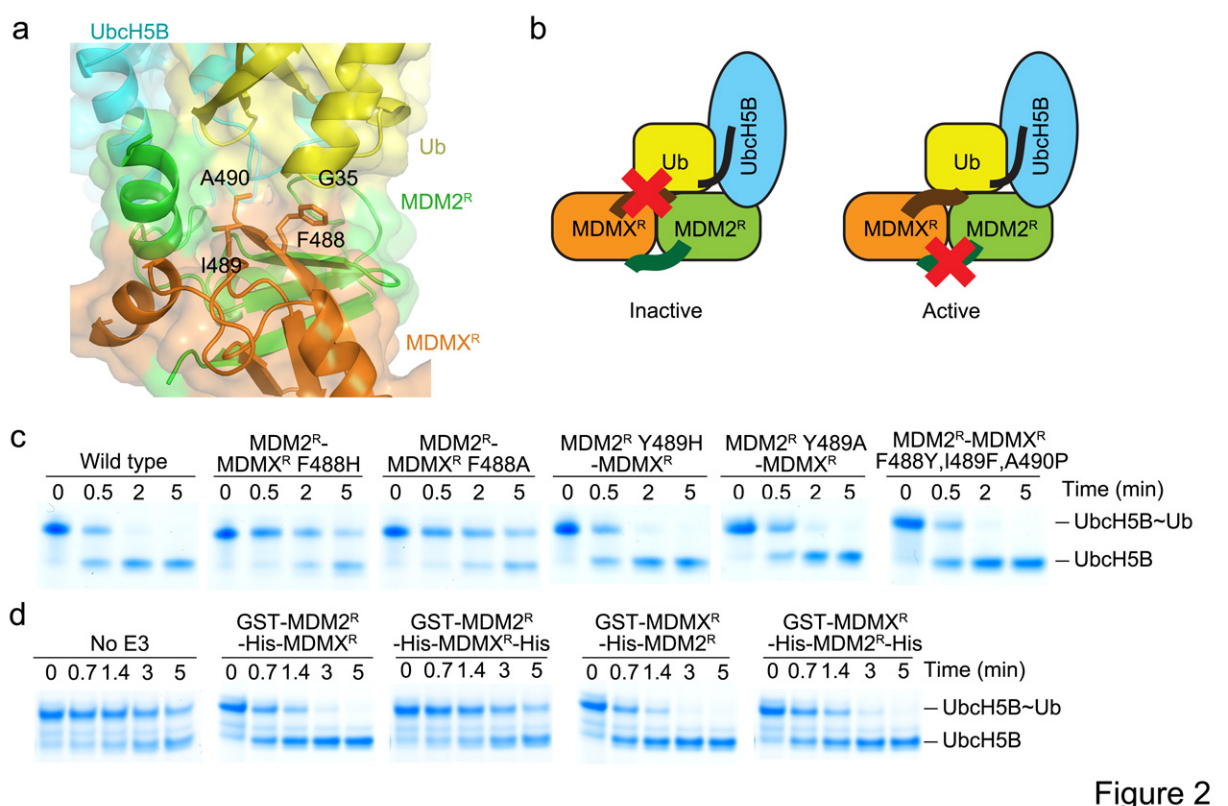
a
UbcH5B
Ub
A490
G35
MDM2R
F488
I489
MDMXR
b
Ub
UbcH5B
MDMXR
MDM2R
Inactive
Ub
UbcH5B
MDMXR
MDM2R
Active
c
Wild type
MDM2R-MDMXR F488H
MDM2R-MDMXR F488A
MDM2R Y489H -MDMXR
MDM2R Y489A -MDMXR
MDM2R-MDMXR F488Y,I489F,A490P
0 0.5 2 5
Time (min)
UbcH5B~Ub
UbcH5B
d
No E3
GST-MDM2R -His-MDMXR
GST-MDM2R -His-MDMXR-His
GST-MDMXR -His-MDM2R
GST-MDMXR -His-MDM2R-His
0 0.7 1.4 3 5
Time (min)
UbcH5B~Ub
UbcH5B

Figure 2

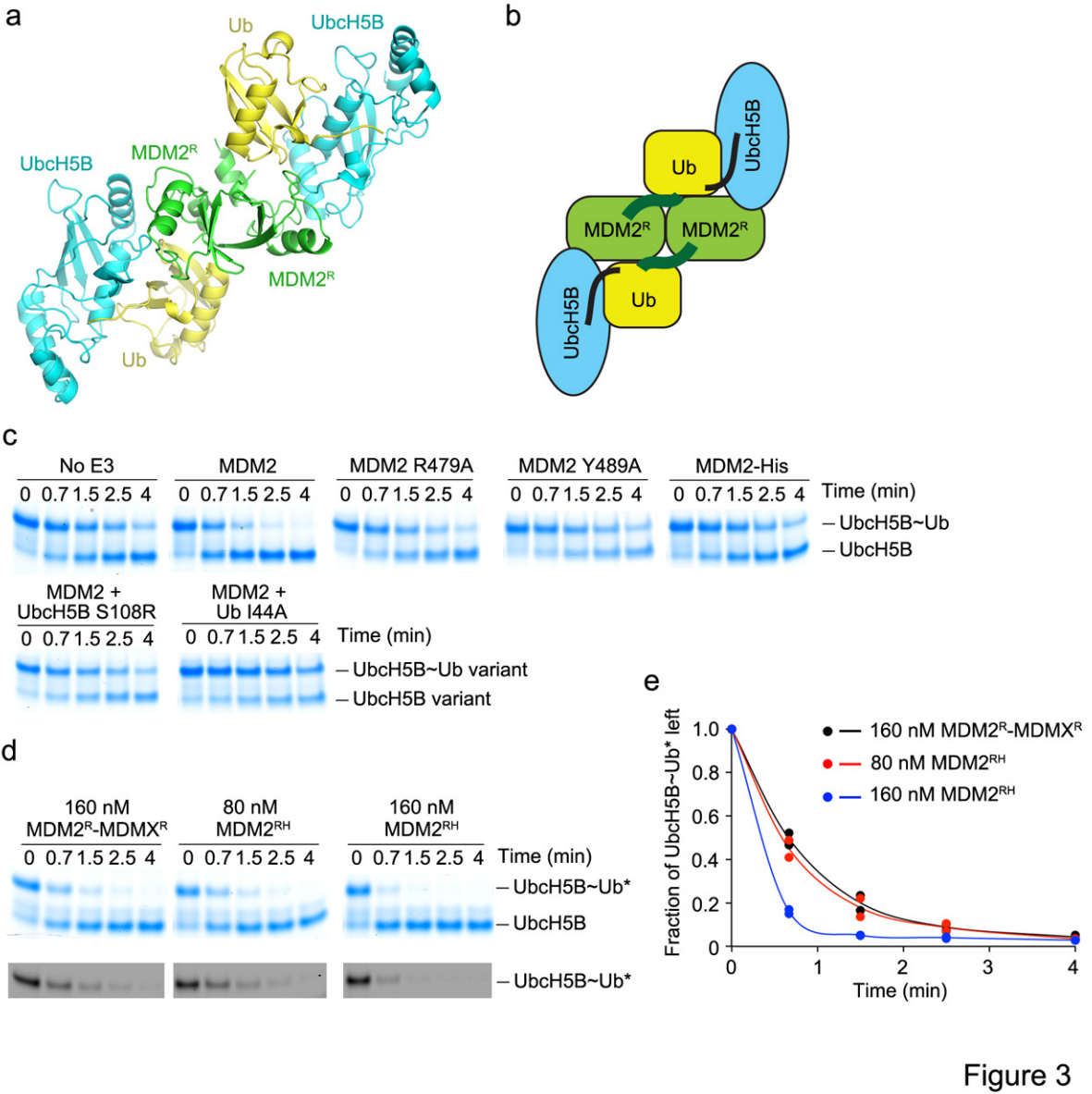
a
Ub
UbcH5B
UbcH5B
MDM2R
MDM2R
Ub
b
UbcH5B
Ub
MDM2R
MDM2R
Ub
UbcH5B
c
No E3
MDM2
MDM2 R479A
MDM2 Y489A
MDM2-His
0 0.7 1.5 2.5 4
Time (min)
– UbcH5B~Ub
– UbcH5B
MDM2 + UbcH5B S108R
MDM2 + Ub I44A
– UbcH5B~Ub variant
– UbcH5B variant
d
160 nM MDM2R-MDMXR
80 nM MDM2RH
160 nM MDM2RH
– UbcH5B~Ub*
– UbcH5B
– UbcH5B~Ub*
e
160 nM MDM2R-MDMXR
80 nM MDM2RH
160 nM MDM2RH
Fraction of UbcH5B~Ub* left
Time (min)

Figure 3

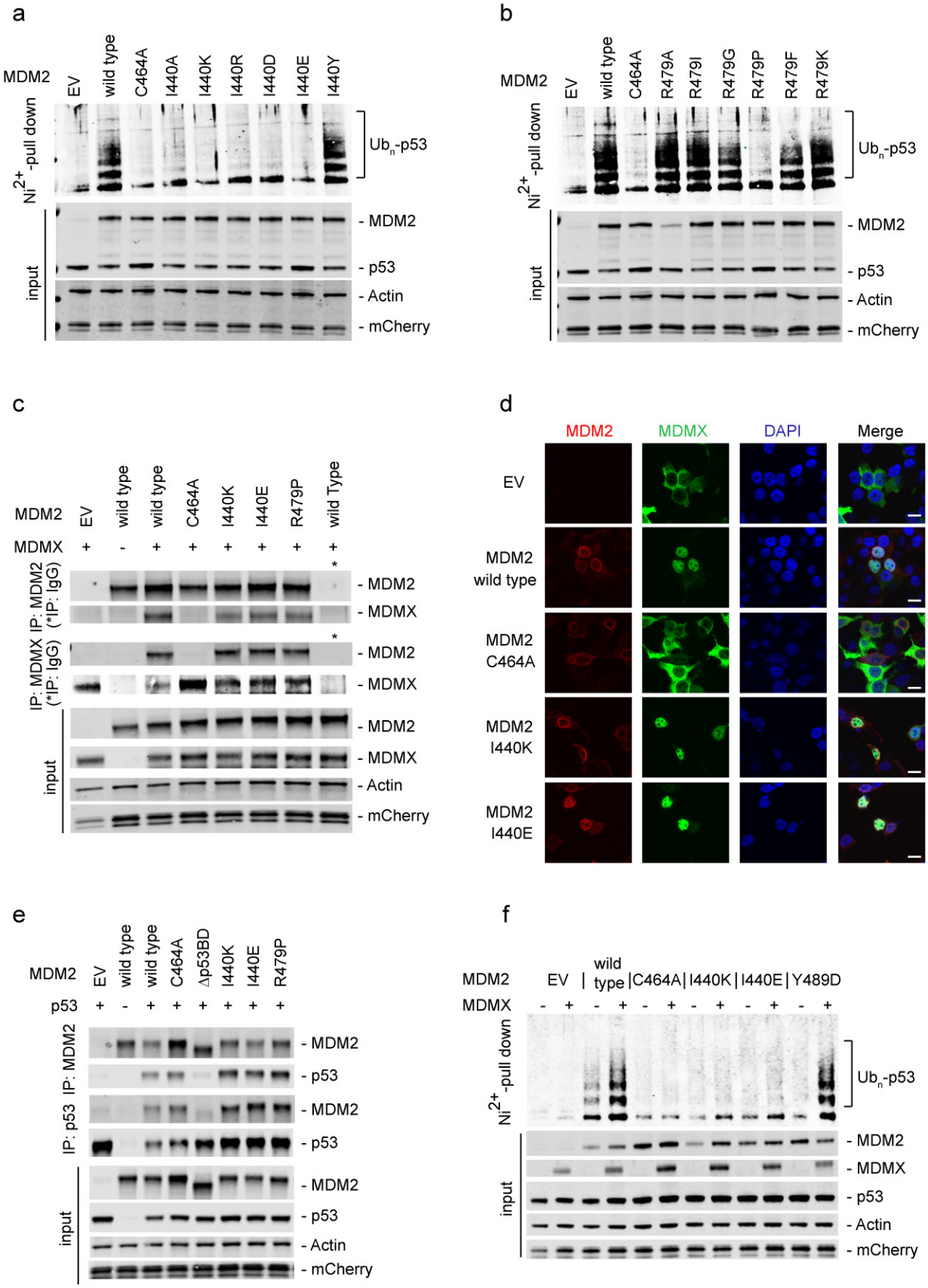
a
MDM2
EV
wild type
C464A
I440A
I440K
I440R
I440D
I440E
I440Y
Ni2+-pull down
Ubn-p53
input
- MDM2
- p53
- Actin
- mCherry
b
MDM2
EV
wild type
C464A
R479A
R479I
R479G
R479P
R479F
R479K
Ni2+-pull down
Ubn-p53
input
- MDM2
- p53
- Actin
- mCherry
c
MDM2
EV
wild type
wild type
C464A
I440K
I440E
R479P
wild Type
MDMX
+ - + + + + + +
IP: MDM2 (*IP: IgG)
- MDM2
- MDMX
IP: MDMX (*IP: IgG)
- MDM2
- MDMX
input
- MDM2
- MDMX
- Actin
- mCherry
d
MDM2
MDMX
DAPI
Merge
EV
MDM2 wild type
MDM2 C464A
MDM2 I440K
MDM2 I440E
e
MDM2
EV
wild type
wild type
C464A
Δp53BD
I440K
I440E
R479P
p53
+ - + + + + + +
IP: MDM2
- MDM2
- p53
IP: p53
- MDM2
- p53
input
- MDM2
- p53
- Actin
- mCherry
f
MDM2
EV
wild type
C464A
I440K
I440E
Y489D
MDMX
- + - + - + - + - + - +
Ni2+-pull down
Ubn-p53
input
- MDM2
- MDMX
- p53
- Actin
- mCherry

Figure 4

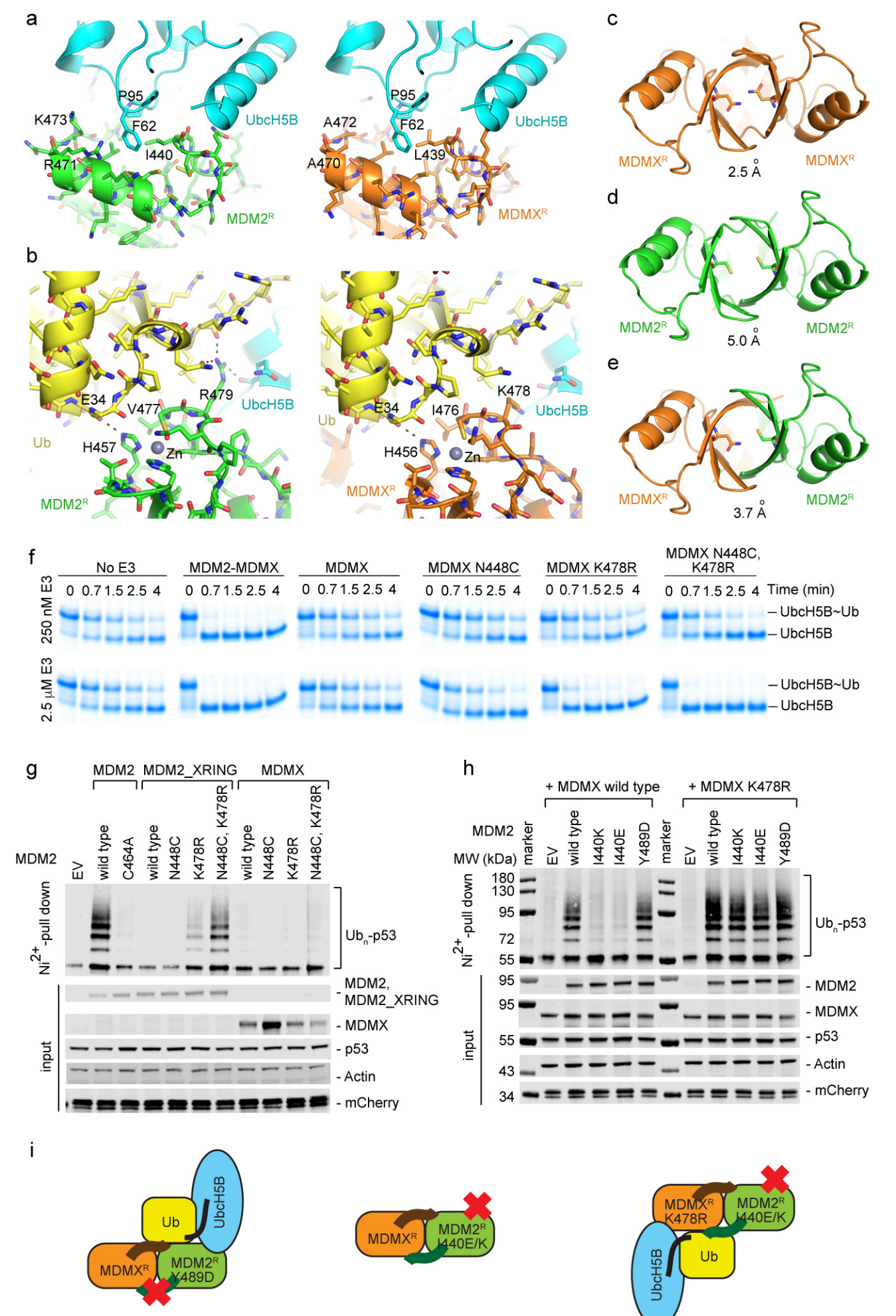
a
P95
K473
F62
UbcH5B
I440
R471
MDM2R
A472
A470
L439
MDMXR
b
E34
V477
R479
UbcH5B
Ub
H457
Zn
MDM2R
K478
I476
H456
c
MDMXR
2.5 Å
d
MDM2R
5.0 Å
e
3.7 Å
f
No E3
MDM2-MDMX
MDMX
MDMX N448C
MDMX K478R
MDMX N448C, K478R
0 0.7 1.5 2.5 4
Time (min)
250 nM E3
2.5 μM E3
UbcH5B~Ub
UbcH5B
g
MDM2
MDM2_XRING
MDMX
EV
wild type
C464A
N448C
K478R
N448C, K478R
Ni2+-pull down
Ubn-p53
input
- MDM2, MDM2_XRING
- MDMX
- p53
- Actin
- mCherry
h
+ MDMX wild type
+ MDMX K478R
MW (kDa)
marker
I440K
I440E
Y489D
180
130
95
72
55
43
34
i
Ub
UbcH5B
MDMXR
MDM2R Y489D
MDM2R I440E/K
MDMXR K478R
Figure 5

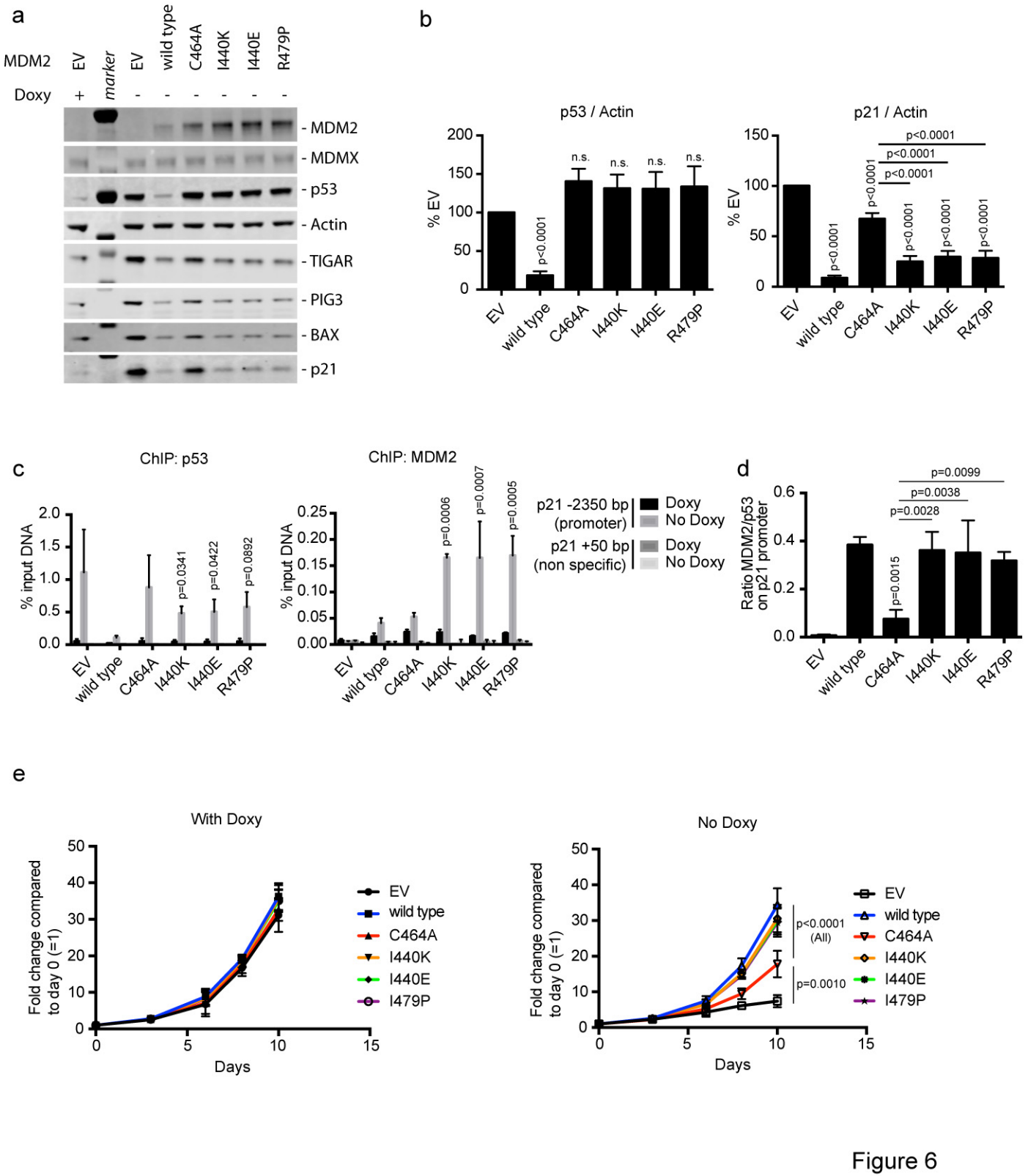
a
MDM2
EV
marker
EV
wild type
C464A
I440K
I440E
R479P
Doxy
+
-
- MDM2
- MDMX
- p53
- Actin
- TIGAR
- PIG3
- BAX
- p21
b
p53 / Actin
% EV
n.s.
p<0.0001
EV
wild type
C464A
I440K
I440E
R479P
p21 / Actin
p<0.0001
c
ChIP: p53
% input DNA
p=0.0341
p=0.0422
p=0.0892
ChIP: MDM2
p=0.0006
p=0.0007
p=0.0005
p21 -2350 bp (promoter)
p21 +50 bp (non specific)
Doxy
No Doxy
d
Ratio MDM2/p53 on p21 promoter
p=0.0099
p=0.0038
p=0.0028
p=0.0015
e
With Doxy
Fold change compared to day 0 (=1)
Days
EV
wild type
C464A
I440K
I440E
I479P
No Doxy
p<0.0001 (All)
p=0.0010

Figure 6

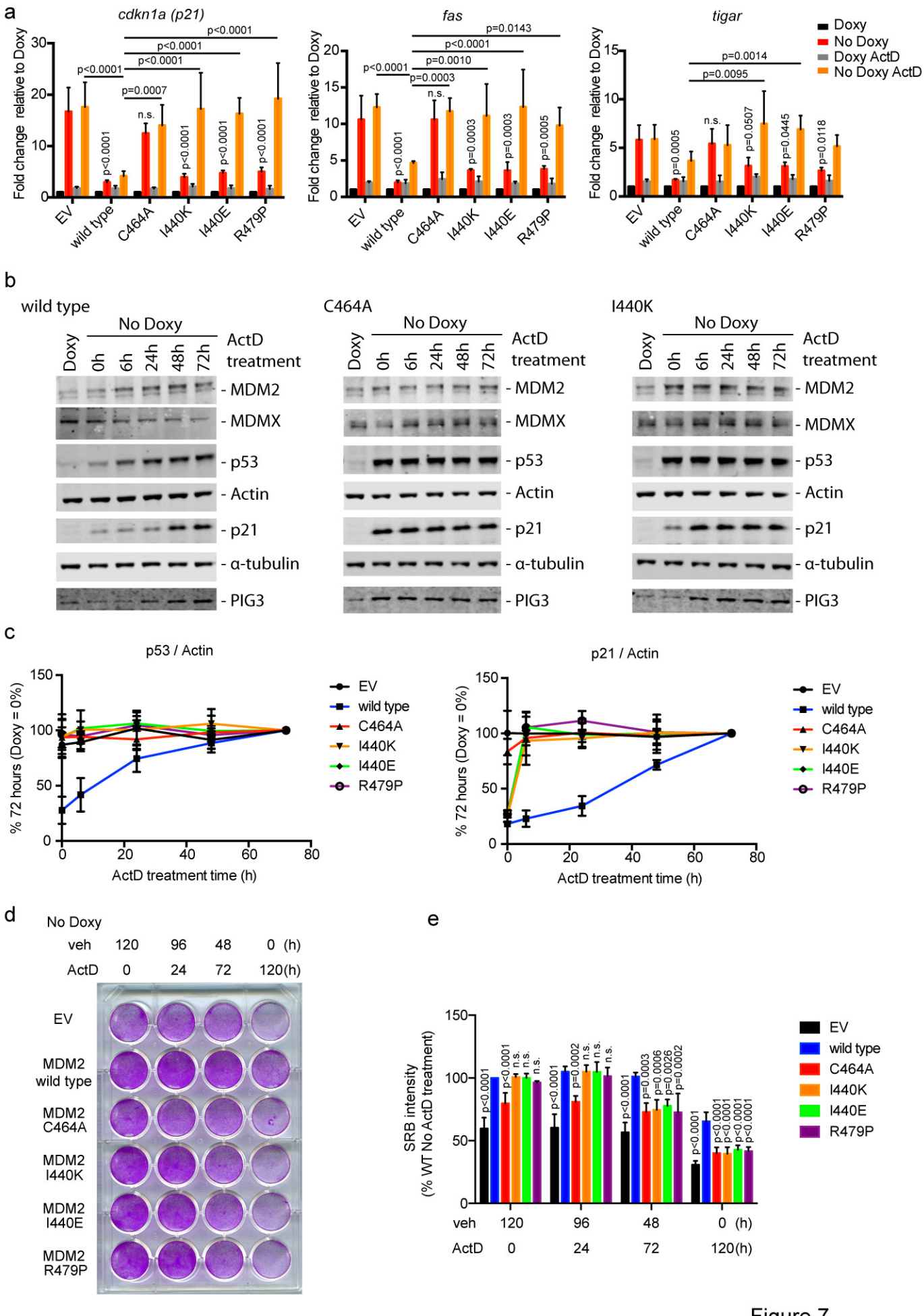
a
cdkn1a (p21)
fas
tigar
Fold change relative to Doxy
Doxy
No Doxy
Doxy ActD
No Doxy ActD
EV
wild type
C464A
I440K
I440E
R479P
b
wild type
C464A
I440K
No Doxy
Doxy
0h
6h
24h
48h
72h
ActD treatment
- MDM2
- MDMX
- p53
- Actin
- p21
- α-tubulin
- PIG3
c
p53 / Actin
p21 / Actin
% 72 hours (Doxy = 0%)
ActD treatment time (h)
d
No Doxy
veh 120 96 48 0 (h)
ActD 0 24 72 120(h)
EV
MDM2 wild type
MDM2 C464A
MDM2 I440K
MDM2 I440E
MDM2 R479P
e
SRB intensity (% WT No ActD treatment)

Figure 7